A generalized Black–Scholes option pricing model and investor sentiment

Kwangwon Ahn[a,b], Minhyuk Jeong[a,b], Biao Yang[c,*]

[a] *Department of Industrial Engineering, Yonsei University, South Korea*

[b] *Center for Finance and Technology, Yonsei University, South Korea*

[c] *Antai College of Economics and Management, Shanghai Jiao Tong University, China*

* *Corresponding author: biao.yang@sjtu.edu.cn (B.Y.)*

Preliminary and incomplete

Second draft: January 2025

Abstract

This paper extends the Black–Scholes (BS) option pricing model using the generalized solution to the heat equation. We derive a closed-form solution for a generalized BS model, which enhances the standard call option price by introducing two additional augments interpreted as factors associated with investor sentiment toward the underlying asset. Our model outperforms the standard BS model in both in-sample fit and out-of-sample prediction using the S&P 500 call option data. Robustness tests corroborate our results. Further analysis shows that the new parameters effectively capture investor expectations, offering improved explanations for deviations of market prices from the BS model.

Keywords: Option pricing; Investor sentiment; Generalized Black–Scholes model; Expectation of return; Expectation of volatility

1. Introduction

The seminal work of Black and Scholes (1973) laid the foundation of modern option pricing theory. Their theory remains the fundamental workhorse in the derivative world, affecting academics and practitioners alike; however, its empirical performance faces restrictive assumptions. Consequently, researchers have proposed various option pricing models based on more realistic assumptions and theories for the past five decades, attempting to correct the mispricing of the standard Black–Scholes (BS) model.[1]

This paper extends the standard BS option pricing framework and derives a closed-form solution for a generalized pricing model. Specifically, we transform the partial differential equation (PDE) of option price to the heat equation, in which the generalized solution has been newly developed (Choi et al. 2017), to derive a generalized BS (GBS) pricing model. Compared to the BS model, our analytic pricing formula contains additional pricing factors. In particular, our GBS model's option price is a linear combination of the BS implied price and the two terms capturing investor sentiment related to risk-neutral (RN) skewness and kurtosis. We then refine our GBS pricing model using a judicious parametrization of additional pricing terms to show that they are likely related to investor sentiment. The corresponding parameters are interpreted as implied sentiment factors because they reflect investors' perception of future return prospects, specifically the expectation of future return and its volatility.

The GBS model proposed in the current study is a novel modification to the standard BS model. It directly incorporates the impact of investor sentiment into the theoretical pricing model, providing a new, economically meaningful way to fix mispricing in the existing option models. The standard BS model can be viewed as a special case of the GBS model, wherein

[1] For instance, volatility smile, which market professionals initially identified, is among the early empirical challenges of the validity of the BS assumptions, which led to a broader question of how to correct the BS pricing bias. See Rubinstein (1976) for an early study concerning the *smile*.

investor sentiment plays no role in pricing options. The empirical results confirm our interpretation. The estimated sentiment-related parameters, which improve the accuracy of option pricing, are significantly correlated with investor sentiment represented by the expectations of future returns and volatility. Thus, our empirical analysis provides direct evidence that the GBS model can reflect investor sentiment to option pricing, and investor sentiment may serve as a significant pricing determinant in the derivative market, not just in the stock market.

We conduct in-sample fit and out-of-sample prediction tests using the S&P 500 index call option prices to determine if our proposed pricing model and the corresponding interpretations can be empirically validated. The results corroborate that the GBS model consistently outperforms the BS model with much smaller pricing and prediction errors. We estimate the parameters through four approaches to compare the relative pricing errors of the two models considered for the in-sample pricing fit. The dominant advantage of the GBS model is that the average daily sum of squared errors (SSE) of the GBS model is significantly smaller than that of the BS model over the entire sample period with a 100% win ratio. Following Bakshi et al. (1997), we further divide our option data into 24 categories according to moneyness and maturity. This approach allows us to examine how well the GBS model captures the potential impact of the underlying properties of the option contracts and to confirm the robustness of the in-sample fit and out-of-sample prediction performances. Our out-of-sample prediction performance employs the same estimation methodologies used for in-sample tests, revealing that the GBS model has a better in-sample pricing fit and a stronger predictive power than the BS model. The correlation and regression results in Tables 9–11 show that the new structural parameters in the GBS model are closely related to a popular investor sentiment proxy, confirming our interpretation of the parameters.

Following Black and Scholes (1973), the major innovations in option pricing research comprise three broad areas. First, the models incorporate the stochastic nature of the underlying determinants of option prices. Notably, temporal variations in interest rates and the volatility of underlying assets are important aspects that must be considered in any option pricing model aiming for satisfactory empirical performances.[2] Second, researchers realized that the Gaussian assumption for the underlying asset return distribution might not perfectly align with what they observed in the data. In particular, higher moments, such as skewness and kurtosis, affect the market participants' perception of risk and hence the risk premiums. Alternative distributions and jump components have been proposed to capture the departure from the Gaussian distribution of underlying asset returns and abrupt movements in stock prices.[3] The

[2] Since Merton (1973) developed a stochastic interest rate pricing model for equity options, a large number of studies have followed by further relaxing the restrictive BS assumptions to investigate different markets. To name a few among many others, Amin and Jarrow (1991), pointing out Merton's model cannot be extended to pricing American options due to the lack of a continuum of distinct bonds, propose an alternative approach based on the equivalent martingale measure and stochastic interest rate in Heath et al. (1992) with the application to foreign currency and currency futures options. Amin and Jarrow (1992) further extended their stochastic interest rate option pricing model by including risky asset, and derive the closed-form solutions for European type call and put options on a risky asset, forward and future contracts. They also explore the valuation of an American option whose payoff depends on the term structure of interest rate. Miltersen and Schwartz (1998) further extend this research field to commodity option market, assuming stochastic interest rate as well as convenience yield. Constant volatility, another restrictive assumption of the BS model, has also been challenged. Following Scott (1987), Hull and White (1987) and Wiggins (1987), stochastic volatility is built in option models with substantial pricing and hedging improvement (Bakshi et al. (1997) and Melino and Turnbull (1990, 1991) for currency options). Following largely numerical-analysis-based studies till then, Heston (1993) derives a closed-form solution to European options with stochastic volatility. Amin and Ng (1993) introduce both stochastic volatility and stochastic interest rate in a different approach, assuming the underlying stock price is correlated with consumption growth or market return, and generalizing the consumption based equilibrium of Rubinstein (1976) and Brennan (1979). Bakshi and Chen (1997a,b) studied the valuation and hedging of foreign currency options with the Lucas (1982) two-country model, assuming a stochastic structure for the international economy.

[3] Bates (1991, 1996) derived a pricing model with a jump-diffusion process to test whether an expectation of a market crash existed before 1987 and later combines a stochastic volatility model with a jump-diffusion process by extending the methodology of Stein and Stein (1991) and Heston (1993). Bates (2000) introduced time-varying jump intensity in the jump-diffusion model with stochastic volatility to explain negative skewness implied in index option prices after 1987. Eraker et al. (2003) added a jump component to the volatility process of the stochastic volatility model with jumps, namely a price/volatility cojump model, and Eraker (2004) and Andersen et al. (2015) allowed time-varying jump intensities in this model. Scott (1997) and Bakshi and Chen (1997a) further extended the jump-diffusion model to incorporate both stochastic volatility and the stochastic interest rate to reflect the empirical characteristics of the underlying stock return, such as leptokurtosis, random change of volatility, and negative correlation between stock returns and volatility. Jump risks, especially negative jump risks, implied in option prices can be related to risks of large consumption declines (Backus et al., 2011; Seo and Wachter, 2019); Shaliastovich (2015) showed that jumps in investors' confidence about future growth endogenously affect jump risks in option markets. Some other studies relax the Gaussian assumption by applying the Edgeworth series expansion (Jarrow and Rudd, 1982) or the Gram-Charlier expansion (Corrado and Su 1996). Borland (2002a,b) and Borland and Bouchaud (2004) developed a non-Gaussian stock pricing model by employing a Tsallis distribution of the entropic index to capture the driving noise of

most recent improvements in option pricing research have been made by questioning the full rationality of investors. Ample evidence shows that investors may not be fully rational to the extent that the behavioral aspect of investors helps better account for various empirical observations, including stock returns, insider trading, and mergers and acquisitions.[4]

In particular, a growing body of literature shows that investor sentiment is a key determinant of asset prices. Investor sentiment refers to investors' overall attitude or aggregate belief toward the anticipated price development of a particular security or financial market. Starting from early studies of the general mechanism through which mispricing is formed by investor sentiment (Barberis et al., 1998), substantial research has investigated its effect on the cross-section of stock returns (Baker and Wurgler, 2006). Option prices are strictly hindered by no-arbitrage constraints such as put-call parity regardless of the model employed; therefore, it may be argued that there is little room for behavioral factors, particularly investor sentiment, to play a role in asset return determination. However, since the volatility of the underlying asset is unknown and subject to temporal variation, the option can be considered a speculative instrument of current and future volatilities, potentially leading to irrational investor behavior and mispricing.

Indeed, like the stock market, empirical evidence has documented that sentiment-driven mispricing also exists in the options market (Stein, 1989; Poteshman, 2001). Based on the finding that the risk-neutral distribution extracted from option prices could reflect investor

---

the underlying price. McCauley and Gunaratne (2003) used the exponential distribution generated from a Fokker-Planck equation instead to capture the probability of extreme outcomes.

[4] Traditional studies believe that the trading behavior of unsophisticated investors can be ignored because their trades are random and thus cancel each other out or are exploited by competitive rational arbitrageurs who drive the asset prices back to their fundamentals; however, noise trading and various limits to arbitrage can significantly drive the market price away from the fundamental value and reduce the profit opportunity for arbitrageurs (De Long et al., 1990; Shleifer and Vishny, 1997). From a behavioral finance perspective, Polkovnichenko and Zhao (2013) and Baele et al. (2019) provided nonexperimental evidence of probability weighting implied in option prices, which is commonly observed in lab experiments, using the rank-dependent expected utility and the cumulative prospect theory utility, respectively.

sentiment, researchers have recently attempted a new route to the relationship between investor sentiment and the pricing behavior in the options market.[5] The risk-neutral skewness is determined by the slope of the pricing kernel (Aït-Sahalia and Lo, 1998; Aït-Sahalia and Lo, 2000); therefore, a significant relationship between investor sentiment and the risk-neutral skewness would suggest that investor sentiment might affect option prices. Han (2008) tested the relationship of risk-neutral skewness with three sentiment proxies, namely the bull-bear spread, the net position of large speculators, and the valuation error of the index proposed by Sharpe (2002). The research showed that when investors are bearish, the risk-neutral skewness is more negative and the volatility smile deepens; when investors turn bullish, skewness becomes less negative and the volatility smile flattens. Han (2008) concluded that investor sentiment is a key determinant of option prices, but existing popular rational models, including those with stochastic volatility, stochastic volatility with jumps, or asymmetric jumps, cannot account for the impact of investor sentiment.

Existing studies primarily attempt to relate empirical sentiment proxies with certain features of option prices, such as risk-neural skewness and kurtosis, to draw some indirect evidence on the pricing implications of investor sentiment, largely because theoretical option pricing models cannot accommodate the impact of investor sentiment in isolation. In contrast, our paper directly admits investor sentiment to the analytic option pricing formula and provides empirical support that considering investor sentiment substantially reduces the pricing errors in the options market.

The rest of the paper proceeds as follows. Section 2 explains how we derive a closed-form solution for our GBS option pricing model and the interpretation of the two newly incorporated

[5] Earlier studies (Jarrow and Rudd, 1982; Corrado and Su, 1996) built up non-Gaussian option pricing models with a correction part incorporating skewness and kurtosis without connecting to investor sentiment or any other behavioral factors.

key parameters. Section 3 introduces the S&P 500 call option dataset and provides descriptive information. Section 4 presents the in-sample fit and out-of-sample prediction performances and discusses the economic meaning of the GBS model. Finally, Section 5 concludes.

2. Theoretical framework

2.1. Standard BS model

Black and Scholes (1973) showed how to solve a PDE for the option price with the heat equation. We summarize the key steps here because part of the derivation is used to obtain the GBS pricing equation.[6]

The following PDE governs the call option price:

$$\frac{\partial C}{\partial t} + \frac{1}{2}\sigma^2 S^2 \frac{\partial^2 C}{\partial S^2} + rS\frac{\partial C}{\partial S} - rC = 0, \tag{1}$$

with the boundary condition

$$C(T, S) = \max(S - K, 0),$$

where K and T are the strike price and the time when the option matures, respectively. Through the change of variables, we obtain:

$$C(t, S) = Ke^{-\frac{1}{2}(k-1)x - \frac{1}{4}(k+1)^2\tau} u(v, x),$$

where

$$x = \ln\left(\frac{S}{K}\right), \qquad v = \frac{\sigma^2}{2}(T - t), \qquad k = \frac{2r}{\sigma^2}.$$

Then, $u(v, x)$ satisfies the heat equation

[6] Further details are presented in Appendix A.

$$\frac{\partial u}{\partial v} = \frac{\partial^2 u}{\partial x^2}$$

with the boundary condition

$$\phi(x) = u(0, x) = \max\left[e^{(1-\alpha)x} - e^{-\alpha x}, 0\right].$$

Appendix A shows the detailed procedure for solving the solution to the heat equation:

$$u(v, x) = \frac{1}{\sqrt{4\pi v}} \int_{-\infty}^{\infty} \phi(y) e^{-\frac{(x-y)^2}{4v}} dy. \tag{2}$$

Thus, the final solution to the price of a call option is

$$C_{BS}(t, S) = S\mathrm{N}(d_1) - Ke^{-r(T-t)}\mathrm{N}(d_2)$$

where

$$d_1 = \frac{\ln(S/K) + (r + \sigma^2/2)(T-t)}{\sigma\sqrt{T-t}},$$

$$d_2 = \frac{\ln(S/K) + (r - \sigma^2/2)(T-t)}{\sigma\sqrt{T-t}}.$$

2.2. Generalized BS model

Two alternative approaches exist to reach a generalized solution to the BS PDE; both correspond to the Taylor expansion and the Hermite polynomial expansion. We prove these two approaches are equivalent and lead to the same general BS PDE solution, which is a summation of an infinite series of functions; therefore, we only provide a few of the first components to obtain a simplified version of the GBS solution.

Choi et al. (2017) showed a generalized solution to the heat equation. Starting from Eq. (2), we define

$$\theta(v, x) \equiv -\frac{\partial u}{\partial x}, \qquad \eta(v, x) \equiv -\frac{\partial \theta}{\partial x}, \qquad \chi(v, x) \equiv -\frac{\partial \eta}{\partial x}.$$

Here, $\theta(v,x)$, $\eta(v,x)$, and $\chi(v,x)$ are the negative first-order, second-order, and third-order derivatives of $u(v,x)$, respectively.[7] It is straightforward to prove that all $u(v,x)$, $\theta(v,x)$, $\eta(v,x)$, and $\chi(v,x)$ satisfy the heat equations as specified below:

$$\frac{\partial u}{\partial v}=\frac{\partial^2 u}{\partial x^2},\qquad \frac{\partial \theta}{\partial v}=\frac{\partial^2 \theta}{\partial x^2},\qquad \frac{\partial \eta}{\partial v}=\frac{\partial^2 \eta}{\partial x^2},\qquad \frac{\partial \chi}{\partial v}=\frac{\partial^2 \chi}{\partial x^2}.$$

We then linearly combine the four terms to obtain the generalized solution to the heat equation. Here, γ, λ, κ, and ω are introduced as coefficients and are assumed to be constants for simplicity,[8]

$$\varphi(v,x)=\gamma u(v,x)+\lambda\theta(v,x)+\kappa\eta(v,x)+\omega\chi(v,x). \tag{3}$$

For any coefficients $\{\gamma,\lambda,\kappa,\omega\}$, the function $\varphi(v,x)$ satisfies the heat equation

$$\frac{\partial \varphi}{\partial v}=\frac{\partial^2 \varphi}{\partial x^2}.$$

However, this does not mean that these four coefficients are free parameters. They must be constrained to let the function $\varphi(v,x)$ satisfy the boundary condition

$$\lim_{v\to 0}\varphi(v,x)=\max\left[e^{\frac{1}{2}(k+1)x}-e^{\frac{1}{2}(k-1)x},0\right].$$

Appendix B shows that the following constraints hold for the four coefficients:

$$\gamma=1,\qquad \lambda=\frac{k^2-1}{4}\omega,\qquad \kappa=k\omega,$$

where ω is a free parameter; thus, the degree of freedom for these four coefficients is only one.

[7] We include the negative sign here to be consistent with Choi et al. (2017). Without the negative sign, the conclusions still hold.

[8] One can keep taking the derivative and include infinitely many of them to obtain the general solution of the heat equation. We focus only on the first four terms to maintain a simple and intuitive solution.

The generalized solution to the heat equation satisfies the boundary condition and can be greatly simplified as

$$\varphi(v,x) = u(v,x) + \frac{\omega x}{2v}\frac{1}{\sqrt{4\pi v}}e^{-\frac{x^2}{4v}}.$$

Then, we can recover the generalized solution to the BS PDE as follows:

$$\begin{aligned} C_{GBS}(t,S) = {} & S\mathrm{N}(d_1) - Ke^{-r(T-t)}\mathrm{N}(d_2) \\ & + K\omega\frac{\ln(S/K)}{\sigma^2(T-t)}\frac{1}{\sqrt{2\pi\sigma^2(T-t)}}e^{-\frac{d^2}{2}-r(T-t)}. \end{aligned} \tag{4}$$

The above approach corresponds to the Taylor expansion because we use a series of derivatives. By adding derivatives and coefficients, the GBS solutions would have more components and be more complicated. In an alternative approach, Choi and Choi (2018) provided a generalized solution to the BS PDE through the Hermite polynomial expansion, proving that this solution satisfies both the BS PDE and the boundary condition,[9]

$$C_{GBS}(t,S) = C_{BS}(t,S) + \sum_{k=0}^{\infty}\zeta_k c_{2k+1}(t,S) \tag{5}$$

where

$$c_k(t,S) = \frac{1}{\left(\sigma\sqrt{T-t}\right)^{k+1}}H_k\left(\frac{\ln(S/K)}{\sigma\sqrt{T-t}}\right)\frac{1}{\sqrt{2\pi}}e^{-\frac{d_2^2}{2}-r(T-t)}.$$

Here, $H_k(\cdot)$ is the probabilist's Hermite polynomials defined as

[9] Choi and Choi (2018) provided a general solution to the BS PDE valid for $S \in (0,\infty)$ in a more general form:

$$C_{GBS}(t,S) = C_{BS}(t,S) + \sum_{k=1}^{\infty}\xi_k c_k(t,S).$$

We only consider the odd terms because we find that $\lim_{t\to T} c_k(t,S) = \infty$ when $S = K$ and k is even. We provide the proof in Appendix C.

$$H_k(x) = (-1)^k e^{\frac{x^2}{2}} \frac{d^n}{dx^n} e^{-\frac{x^2}{2}}.$$

If we consider the first two terms, then the GBS solution is

$$C_{GBS}(t,S) = C_{BS}(t,S) + \zeta_0 c_1(t,S) + \zeta_1 c_3(t,S),$$

where

$$c_1(t,S) = \frac{1}{\left(\sigma\sqrt{T-t}\right)^2} \frac{\ln(S/K)}{\sigma\sqrt{T-t}} \frac{1}{\sqrt{2\pi}} e^{-\frac{d_2^2}{2} - r(T-t)}, \text{and}$$

$$c_3(t,S) = \frac{1}{\left(\sigma\sqrt{T-t}\right)^4} \left(\left[\frac{\ln(S/K)}{\sigma\sqrt{T-t}} \right]^3 - 3 \frac{\ln(S/K)}{\sigma\sqrt{T-t}} \right) \frac{1}{\sqrt{2\pi}} e^{-\frac{d_2^2}{2} - r(T-t)}.$$

This general solution has two free parameters, ζ_0 and ζ_1. The GBS solution in Eq. (4) is a special case of that in Eq. (5) with $\zeta_0 = \omega K$ and $\zeta_1 = 0$; thus, these two approaches are equivalent and result in the same GBS solution.

Figure 1 shows the GBS call option price as a function of the underlying stock price S. In this figure, the GBS price only includes c_1, i.e.,

$$C_{GBS}(t,S) = C_{BS}(t,S) + \zeta_0 c_1(t,S).$$

(1) GBS and BS prices are always the same when $S = K$. (2) When ζ_0 is negative, the GBS price is higher than the BS price at out-of-the-money (OTM) calls and lower than the BS price at in-the-money (ITM) calls; the opposite is true when ζ_0 is positive.

[Insert Figure 1 here]

Next, we examine the GBS price with two additional terms. Figure 2 shows the price as a function of the underlying price:

$$C_{GBS}(t,S) = C_{BS}(t,S) + \zeta_0 c_1(t,S) + \zeta_1 c_3(t,S).$$

The findings from Figure 2 are threefold. First, the GBS option price is much more sensitive

to the second term than the first term; thus, a reasonable parameter choice requires $\zeta_1 \ll \zeta_0$. Second, a positive ζ_1 increases GBS price at OTM calls but decreases it at deep OTM calls. Third, a positive ζ_1 decreases GBS price at ITM calls but increases it at deep ITM calls.[10]

[Insert Figure 2 here]

2.3. Risk-neutral skewness and kurtosis in the GBS model

According to Bakshi et al. (2003), the risk-neutral (RN) skewness and kurtosis of an underlying stock return over the period $(t, t+\tau)$ can be recovered using OTM European option prices as follows:

$$\text{SKEW}(t,\tau) \equiv \frac{e^{r\tau}W(t,\tau) - 3\mu(t,\tau)e^{r\tau}V(t,\tau) + 2\mu(t,\tau)^3}{[e^{r\tau}V(t,\tau) - \mu(t,\tau)^2]^{3/2}} \tag{6}$$

$$\begin{aligned}&\text{KURT}(t,\tau)\\ &\equiv \frac{e^{r\tau}X(t,\tau) - 4\mu(t,\tau)e^{r\tau}W(t,\tau) + 6e^{r\tau}\mu(t,\tau)^2V(t,\tau) - 3\mu(t,\tau)^4}{[e^{r\tau}V(t,\tau) - \mu(t,\tau)^2]^2}\end{aligned} \tag{7}$$

where

$$V(t,\tau) \equiv \int_{S(t)}^{\infty} \frac{2\left(1 - \ln\frac{K}{S(t)}\right)}{K^2} C(t,S(t);\tau,K)dK + \int_0^{S(t)} \frac{2\left(1 + \ln\frac{S(t)}{K}\right)}{K^2} P(t,S(t);\tau,K)dK$$

$$W(t,\tau) = \int_{S(t)}^{\infty} \frac{6\ln\frac{K}{S(t)} - 3\left(\ln\frac{K}{S(t)}\right)^2}{K^2} C(t,S(t);\tau,K)dK$$

$$- \int_0^{S(t)} \frac{6\ln\frac{S(t)}{K} + 3\left(\ln\frac{S(t)}{K}\right)^2}{K^2} P(t,S(t);\tau,K)dK$$

[10] These are because c_3 is a cubic function of $\ln(S/K)$.

$$X(t,\tau) = \int_{S(t)}^{\infty} \frac{12\left(\ln\frac{K}{S(t)}\right)^2 - 4\left(\ln\frac{K}{S(t)}\right)^3}{K^2} C(t,S(t);\tau,K)dK$$

$$+ \int_{0}^{S(t)} \frac{12\left(\ln\frac{S(t)}{K}\right)^2 + 4\left(\ln\frac{S(t)}{K}\right)^3}{K^2} P(t,S(t);\tau,K)dK$$

and

$$\mu(t,\tau) = e^{r\tau}\left[1 - \frac{1}{2}V(t,\tau) - \frac{1}{6}W(t,\tau) - \frac{1}{24}X(t,\tau)\right] - 1. \quad (8)$$

Here, $C(t,S(t);\tau,K)$ and $P(t,S(t);\tau,K)$ are call and put option prices at t with underlying price $S(t)$ given time-to-maturity τ $(= T - t)$ and strike price K. This nonparametric method is usually used to obtain RN skewness and kurtosis through empirical option prices; however, we can theoretically extract the model-implied RN skewness and kurtosis because we have an analytic solution for the option prices through the GBS model.

Eq. (8) is based on an approximation by Bakshi et al. (2003); however, instead of using an approximation, we can use the same logic for deriving V, W, and X to get the exact solution for μ,[11]

[11] A simple proof is here. According to Eq. (3) in Bakshi et al. (2003),

$$E_t^*\left[e^{-r\tau}H\left(S(t+\tau)\right)\right]$$
$$= \left(H(\bar{S}) - \bar{S}H_S(\bar{S})\right)e^{-r\tau} + H_S(\bar{S})S(t) + \int_{\bar{S}}^{\infty} H_{SS}(K)C(t,S(t);\tau,K)dK + \int_{0}^{\bar{S}} H_{SS}(K)P(t,S(t);\tau,K)dK.$$

Let $H\left(S(t+\tau)\right) = \ln\frac{S(t+\tau)}{S(t)}$ and $\bar{S} = S(t)$. We then get

$$\mu(t,\tau) \equiv E_t^*\left[\ln\frac{S(t+\tau)}{S(t)}\right]$$
$$= e^{r\tau}\left[-e^{-r\tau} + 1 + \int_{S(t)}^{\infty} -\frac{1}{K^2}C(t,S(t);\tau,K)dK + \int_{0}^{S(t)} -\frac{1}{K^2}P(t,S(t);\tau,K)dK\right]$$
$$= e^{r\tau}\left[1 - \int_{S(t)}^{\infty}\frac{1}{K^2}C(t,S(t);\tau,K)dK - \int_{0}^{S(t)}\frac{1}{K^2}P(t,S(t);\tau,K)dK\right] - 1.$$

$$\mu(t,\tau) = e^{r\tau}\left[1 - \int_{S(t)}^{\infty} \frac{1}{K^2} C(t,S(t);\tau,K)dK - \int_{0}^{S(t)} \frac{1}{K^2} P(t,S(t);\tau,K)dK\right] - 1. \quad (9)$$

This formula simplifies the calculation compared to Eq. (8).

Our GBS formula is an additive function with the BS formula as one component; therefore, we first examine the implied skewness and kurtosis given by the BS formula. Based on the BS model's underlying assumption, we expect that the implied skewness should be 0 and the implied kurtosis should be 3, which is the case.

2.3.1. Implied skewness and kurtosis of the BS model.

PROPOSITION 2.1: *The model-implied RN skewness and kurtosis for the standard BS model are 0 and 3, respectively.*

Proof: See Appendix D.

Proposition 2.1 is a well-known result, which can be easily proven using the previously described method. The results support the underlying assumption of the BS model. That is, stock returns follow geometric Brownian motion, and its RN distribution is Gaussian with zero skewness and kurtosis equals three. This outcome validates the approach provided by Bakshi et al. (2003).

2.3.2. Implied skewness and kurtosis of the GBS model.

Implied RN skewness and kurtosis become quite complicated under GBS. Consider the following GBS formula with two components:

$$C_{GBS}(t,S) = C_{BS}(t,S) + \zeta_0 c_1(t,S) + \zeta_1 c_3(t,S).$$

Due to the put-call parity, the GBS put price is[12]

$$P_{GBS}(t,S) = C_{GBS}(t,S) - S + Ke^{-r\tau} = P_{BS}(t,S) + \zeta_0 c_1(t,S) + \zeta_1 c_3(t,S).$$

The following proposition gives the RN skewness and kurtosis of the GBS model:

PROPOSITION 2.2: *The GBS model-implied RN skewness and kurtosis can be calculated as follows:*

$$\text{SKEW}(t,\tau) = \frac{e^{r\tau}W_{GBS}(t,\tau) - 3\mu_{GBS}(t,\tau)e^{r\tau}V_{GBS}(t,\tau) + 2\mu_{GBS}(t,\tau)^3}{[e^{r\tau}V_{GBS}(t,\tau) - \mu_{GBS}(t,\tau)^2]^{3/2}}$$

$$\text{KURT}(t,\tau)$$

$$= \frac{e^{r\tau}X_{GBS}(t,\tau) - 4\mu_{GBS}(t,\tau)e^{r\tau}W_{GBS}(t,\tau) + 6e^{r\tau}\mu_{GBS}(t,\tau)^2V_{GBS}(t,\tau) - 3\mu_{GBS}(t,\tau)^4}{[e^{r\tau}V_{GBS}(t,\tau) - \mu_{GBS}(t,\tau)^2]^2}.$$

All the variables are given in Appendix D.

Proof: See Appendix D.

These expressions are complicated, and they cannot be simplified further. However, we can show the relation graphically through Figures 3 and 4. First, Figure 3 shows the change in RN skewness and kurtosis concerning ζ_0 if $\zeta_1 = 0$, we have three conclusions. (1) When $\zeta_0 = 0$, the GBS model reduces to the BS model, where we get $\text{SKEW} = 0$ and $\text{KURT} = 3$. (2) RN skewness is decreasing in ζ_0, with it being negative when $\zeta_0 > 0$. And (3) kurtosis is

[12] We can also derive the GBS put price in the following way. Choi and Choi (2018) showed that $c_k(t,S)$ satisfies the BS PDE for any nonnegative integer k. Moreover, the BS PDE for a European put option is given, in the same form as that for a European call option, as

$$\frac{\partial P}{\partial t} + \frac{1}{2}\sigma^2 S^2 \frac{\partial^2 P}{\partial S^2} + rS\frac{\partial P}{\partial S} - rP = 0,$$

with a different boundary condition, where P is the price of a European put option. Accordingly, the generalized solution for a European put option can be derived as

$$P_{GBS}(t,S) = P_{BS}(t,S) + \sum_{k=0}^{\infty} \zeta_k c_{2k+1}(t,S).$$

increasing in ζ_0. In the case of $\zeta_0 > 0$, RN skewness is negative and RN kurtosis is larger than 3, consistent with the stylized facts about asset return distributions (Cont, 2001); therefore, we expect that ζ_0 would be positive, coinciding with the so-called volatility smile of BS model-implied volatilities (Bakshi et al., 2003).[13]

[Insert Figure 3 here]

Next, we examine the relation of ζ_1 with RN skewness and kurtosis while ζ_0 is set to 0. Following the same procedure above, Figure 4 presents the relationship. Again, when $\zeta_1 = 0$, the GBS model reduces to the BS model, which has zero skewness and excess kurtosis. One finding is that RN kurtosis is positively related to ζ_1. Furthermore, RN skewness is negatively related to ζ_1 but the relationship is less significant; thus, we suggest the following postulations with the GBS solution given in Eq. (5). (i) ζ_0 is negatively related to RN skewness and positively related to RN kurtosis. (ii) ζ_1 is positively related to RN kurtosis.

[Insert Figure 4 here]

This section shows that while our GBS model is based on BS model assumptions and derived from BS PDE, our model captures the non-Gaussian RN skewness and kurtosis of the underlying stock returns through the newly added parameters. Han (2008) found a strong relationship between the RN skewness of the index return and investor sentiment. RN skewness is more negative when market sentiment is bearish and vice versa. Therefore, we argue that the new parameters introduced in our GBS model reflect investor sentiment since they affect the RN skewness and kurtosis of the stock return distribution. Section 4 provides empirical evidence that relates our estimated parameters with well-established investor sentiment proxies.

[13] According to Bakshi et al. (2003), a negative RN skewness drives a steeper smile, whereas an increase in RN kurtosis has a negative marginal effect on the implied volatility slopes. However, the impact of a negative RN skewness outweighs that of kurtosis, resulting in the volatility smile.

2.4. Sensitivity analysis

The analysis in this subsection aims to examine: i) how the newly added parameters ζ_0 and ζ_1 affect the GBS call option price and its difference from the BS counterpart; and ii) whether the pricing effects of those parameters in the GBS model are consistent with the interpretation addressed in the previous section. Here, we show the GBS price sensitivity to S, K, ζ_0, and ζ_1.

Figure 5 shows the sensitivity of the GBS and BS prices to S and K for four different combinations of $\zeta_0 \in \{5, -5\}$ and $\zeta_1 \in \{0.05, -0.05\}$. Overall, the GBS and BS prices share similar response patterns in each case, and the GBS-induced adjustment is minor in magnitude, partly due to the parameter values assigned. Overall, (1) ζ_0 has directional effects on the difference between GBS and BS prices. Specifically, positive ζ_0 increases (decreases) the GBS prices of ITM (OTM) call options, and vice versa. In contrast, (2) ζ_1 affects the magnitude more than the direction of the difference between GBS and BS prices. That is, when ζ_1 has the different (same) sign with ζ_0, the directional effect of ζ_0 is amplified (enfeebled).

[Insert Figure 5 here]

We next conduct the sensitivity analysis of the GBS and BS prices concerning the newly introduced parameters, ζ_0 and ζ_1. Figure 6 shows that the GBS price increases (decreases) regarding ζ_0 (ζ_1) for an ITM option and vice versa for an OTM option.

[Insert Figure 6 here]

3. Data

We use a dataset of daily close prices of the S&P 500 call option (TICKER symbol: SPX) from January 3, 2006, to December 31, 2021 (4,028 trading days). SPX is traded on the Chicago Board Options Exchanges, one of the world's most traded European option contracts. It is also

widely used in academia for research on option pricing, including Han (2008), Bakshi et al. (1997), Bakshi et al. (2003), and Dumas et al. (1998). Table 1 describes the features of our dataset.

[Insert Table 1 here]

Following Dumas et al. (1998) and Heston and Nandi (2000), we retrieve the daily option price, the midpoint of the bid-ask quote. For the interest rate, we use LIBOR with maturity of one week, one month, three months, six months, and one year. For each date, these annualized rates are converted to continuously compounded rates and then linearly interpolated to obtain the interest rate for any maturity ranging between one week and one year; this approach follows Han (2008).[14] Most literature on option price fitting requires that the spot stock price be adjusted for discrete dividends; thus, we follow Bakshi et al. (1997) to subtract the S&P 500 index with the present value of its future dividends from the trading day t to the expiration day $t+\tau$.

$$S_i^{ex}(t) = S(t) - \sum_{s=1}^{\tau_i} e^{-r(t,s)s} D(t+s)$$

where $S_i^{ex}(t)$ is the dividend-exclusive S&P 500 index on day t of option i. $S(t)$ is the original S&P 500 index on date t, and τ_i is the time-to-maturity of option i. $r(t,s)$ is the yield-to-maturity from date t to date $t+s$, which is obtained in the previous step using the LIBOR. $D(t)$ is the cash dividend of the S&P 500 index at date t. We use the daily dividend yield to derive the daily cash dividend on day *t*. Specifically, $D(t)$ is calculated by multiplying the effective daily dividend yield by $S(t)$. These are done for each option on each trading day;

[14] The daily LIBOR is collected from the Datastream. Instead of LIBOR, the Treasury bill rates for interpolation can be used, following Bakshi et al. (1997) and Heston and Nandi (2000). The daily Treasury bill rates of different maturity can be hand-collected from the *Wall Street Journal*.

thus, options with different time-to-maturity on the same day may have different spot prices. Each option has a unique market price, spot price, exercise price, time-to-maturity, and interest rate.

In addition to these changes, we applied some filters to the original data following the literature: First, options with time-to-maturity less than one week and more than one year are excluded (Han, 2008). Second, to avoid microstructure-related bias, options with prices less than USD1/8 were excluded (Han, 2008).[15] Third, options with a price that violates the following no-arbitrage conditions are excluded (Han, 2008)

$$S_i^{ex}(t) \geq C_i(t) \geq \max\left\{0, S_i^{ex}(t) - K_i e^{-r(t,T_i-t)(T_i-t)}\right\},$$

where $C_i(t)$ is the price of option i on day t, K_i is the exercise price of option i, and T_i is the time when option i matures. Fourth, following Dumas et al. (1998), options with absolute moneyness higher than 10%, that is, $\left|\frac{S_i^{ex}(t)}{K_i} - 1\right| > 10\%$, are excluded.

3.1. Descriptive statistics

The sample periods are from January 3, 2006, to December 31, 2021, comprising 4,028 trading days, with the total number of observations on daily option prices at 13,701,755 before exclusion. After exclusion, about two-thirds of the option prices are omitted, leaving 4,652,078 total observations. Figure 7 shows the daily number of traded call options in the filtered sample. The maximum number is on December 3, 2021, with 4,508 options traded in the market. On average, 1,154.93 options are traded every day over our sample period.

[Insert Figure 7 here]

[15] Bakshi et al. (1997) excluded options with a price less than USD3/8; we follow Han (2007) as it is more recent and reflects the change in the market micro-structure issues.

Following Bakshi et al. (1997), we divide call option data into different categories. This methodology has two main benefits. First, we can examine the volatility smile by calculating the average implied volatility of each category, thereby investigating whether pricing biases exist in the United States (US) options market. Second, the estimations of implied volatility (or model parameters) for each category help us understand how the pricing performance of an option pricing model can be improved. While Bakshi et al. (1997) obtained 18 categories, we divided the options into 24 for a smoother distribution. We take the following steps for the classification and present the results in Table 2, where we summarize the mean, standard deviation (in parenthesis), total number of option prices in each category, and the subtotal number of each group.

First, according to the moneyness measured by S/K, options are divided into out-of-the-money (OTM) if $S/K < 0.97$, at-the-money (ATM) if $0.97 \leq S/K < 1.03$, and in-the-money (ITM) if $1.03 \leq S/K$. Then, the options in each group are divided into eight categories. Second, according to maturity measured by days-to-expiration, options are divided into short-term (ST) if $T - t < 60$, medium-term (MT) if $60 \leq T - t < 150$, and long-term (LT) if $150 \leq T - t$.

[Insert Table 2 here]

4. Empirical analysis

4.1. Volatility smile

The volatility smile indicates pricing biases across option moneyness. We calculate the average implied volatility for each category to investigate whether such pricing biases exist in the S&P 500 index call options. Table 3 shows the average implied volatilities, and Figure 8 (a) plots the smile shape of the BS model-implied volatilities. This finding is consistent with the implied volatility data provided by the WRDS during the sample period, presented in Figure 8

(b).

[Insert Table 3 here]

[Insert Figure 8 here]

Table 3 and Figure 8 show that the BS model-implied volatility exhibits a smile shape; implied volatility increases sharply as option moneyness deviates from unity, especially for short-term options (i.e., with days-to-expiration smaller than 60). Our data show implied volatility increases in the moneyness for long-term options, which supports Bakshi et al. (1997). A volatility smile indicates that the BS model is indeed subject to mispricing in the S&P 500 call options, especially across moneyness.

4.2. In-sample fit performance

4.2.1. Estimation method

Following Bakshi et al. (1997), we estimate the model parameters by minimizing the sum of squared errors (SSE) to compare the in-sample fit performances of the two models. Specifically, here is our estimation procedures.

First, collect all call option prices from the same day. Denote the parameter set by $\Phi_{i,t} = \{S_i^{ex}(t), K_i, T_i - t, \sigma_t, \zeta_{0,t}, \zeta_{1,t}\}$, and let the model-implied option price be $\hat{C}_{i,t}(\Phi_{i,t})$ and market price be $C_{i,t}$. We define the pricing error of option i on day t as $\epsilon_{i,t}(\Phi_{i,t}) = \hat{C}_{i,t}(\Phi_{i,t}) - C_{i,t}$.

Second, find parameters σ_t, $\zeta_{0,t}$, and $\zeta_{1,t}$ that minimize the SSE defined as

$$SSE_t = \sum_{i=1}^{N} \epsilon_{i,t}^2(\Phi_{i,t}).$$

Here, N is the number of options traded on day t. The objective function, SSE_t, represents

the overall daily pricing bias of the options.[16] We repeat the above procedure for each day. The GBS model has three free parameters: ζ_0, ζ_1, and σ. The BS model has only one free parameter: σ.

We employ three additional classification schemes based on two important option characteristics—moneyness and maturity—to improve the pricing performance and validate the robustness of our model. Following Bakshi et al. (1997), i) options are divided into OTM, ATM, and ITM by moneyness (moneyness-based method); ii) ST, MT, and LT by maturities (maturity-based method); or iii) 9 categories according to both moneyness and maturity (MM-based method). Details of the classification schemes are given below.

1. All option fit: We estimate the parameters for each day using all the option prices; thus, we obtain one set of parameters for each day.
2. Moneyness-based fit: For each day, we divide the options into three groups according to moneyness, i.e., OTM ($S/K < 0.97$), ATM ($0.97 < S/K < 1.03$), and ITM ($S/K > 1.03$). We then estimate the parameters using the option prices in each group and obtain three sets of parameters for each day. We sum the SSE in the three groups to obtain the daily SSE of the BS and GBS models.
3. Maturity-based fit: For each day, we divided the options into three groups according to time-to-maturity, i.e., ST ($T - t < 60$), MT ($60 < T - t < 150$), and LT ($T - t > 150$). We then estimate the parameters using the options prices in each group and obtain three sets of parameters for each day. Finally, we sum the SSE in the three groups to get

[16] For this part of the analysis, we treat all option prices daily as a single group to back out the same model parameter for options with different moneyness levels and maturity. We take this approach to examine the overall impact of investor sentiment on option prices, although it deviates in spirit from our analysis of implied volatility. We later divide the options into different categories according to moneyness and maturity to investigate how well the GBS model captures the structure of the model parameters.

the daily SSE of the BS and GBS models.

4. MM-based fit: For each day, we divide the options into nine groups according to time-to-maturity and moneyness, i.e., OTM-ST, OTM-MT, etc. We then estimate the parameters using the option prices in each group and obtain nine sets of parameters for each day. Finally, we sum the SSE in the nine groups to obtain the daily SSE of the BS and GBS models.

4.2.2. Estimation results

We first estimate the BS and GBS models using all option data daily and obtain the daily estimated parameters and SSE. Table 4 shows the average estimated parameters and SSE and their standard deviations. The estimated volatilities of both models are quite similar. The GBS model reduces the SSE of the BS model by 14% due to the presence of the two additional parameters. In all 4,028 trading days, GBS yielded a smaller SSE than BS, with a 100% win ratio. This outcome is natural because the GBS model is an extension of the BS model, and the BS model is a special case of the GBS model with $\zeta_0 = \zeta_1 = 0$. Later, we verified that GBS outperformed BS in an in-sample fitting and an out-of-sample prediction, indicating that the GBS model is not merely an overfitting.

[Insert Table 4 here]

Figure 9 shows the time series plot of the daily fitted parameters using all options fits. Overall, ζ_1 is not significant in magnitude, and σ of the GBS model is very similar to that of the BS model. The signs of ζ_0 and ζ_1 are consistently positive, implying that the stock return usually has negative RN skewness and positive excess kurtosis; such non-Gaussian features are explained by the additional parameters of GBS (i.e., ζ_0 and ζ_1), which is in line with our postulation.

[Insert Figure 9 here]

We employ the other three additional classification schemes based on moneyness, maturity, and MM. Table 5 shows the average daily SSE of the GBS and BS models. The GBS fits the daily option prices much better than the BS model, with smaller errors. In particular, the SSE of the GBS model is substantially lower when we fit based on maturities than that of the BS model. Strikingly, 77% and 65% of the SSEs are reduced when we turn from the BS model to the GBS model with maturity-based and MM-based estimation methods. This outcome can be explained by the fact that investors have different expectations on the future price change of the underlying stock for different time-to-maturities, and the GBS model can explain such term structures better than the BS model with its generalization terms. The last row shows that the win ratio is always 100%, regardless of the estimation approaches. Such enormous improvements in GBS model pricing accuracy are derived from the additional parameters (and the corresponding pricing terms).

[Insert Table 5 here]

Figure 10 shows the ratio of the daily SSE of the GBS model to that of the BS model; we again find that the GBS model performs best when options are sorted by maturity. Figure 11 shows the differences between the SSEs of the GBS and BS models across the 24 categories when we fit the models using the MM-based estimation. It shows that in all cases, the GBS model outperforms the BS model by a large margin, implying that the GBS model can solve the pricing biases inherent in the BS model.

[Insert Figure 10 here]

[Insert Figure 11 here]

4.2.3. An example of fit performance

We next examine some examples of option fitting and see how GBS improves the goodness

of fit compared to the BS model. We provide an example in Figure 12. Specifically, we use the option prices traded on December 3, 2021, with time-to-maturity equal to 77 days (348 options) with different moneyness. Based on this sample, we estimate the parameters in both the BS and GBS models and plot the actual and fitted prices in Figure 12. The GBS model fits the price much better than the BS model in this example; in particular, the SSE of the BS model in this case is 393,568, whereas the SSE of the GBS is 1,258.

[Insert Figure 12 here]

In addition to maturity-based fitting, we fit option prices based on the same moneyness. Specifically, Figure 13 shows the actual BS and GBS model-fitted prices using sample options on December 3, 2021, with a strike price equal to 4,150 ($K = 4{,}150$) and different maturities (37 options). In this case, the GBS model has a discernable improvement in the fitting performance compared to the BS model: the SSE of the BS model is 8,326, and that of the GBS model is 3,157. In particular, the fitting performance is better for options with a short time-to-maturity. The examples in Figures 12 and 13 confirm that our GBS model outperforms when it fits each group of options with similar maturities; it still outperforms the BS model by a large margin when based on moneyness.

[Insert Figure 13 here]

4.3. Out-of-sample prediction performance

We have shown that the GBS model substantially outperforms the BS model regarding the in-sample pricing fit; however, one may argue that its superior in-sample fit could result from overfitting with more parameters. We compared the out-of-sample prediction performances of the two models to verify that our GBS model has a comparative advantage. The steps are as follows.

First, we estimate the model parameters for each day using the four methods used for in-

sample tests. Second, for each day t, we calculate the predicted option prices using the model parameters estimated for day $t-1$ $(\sigma_{t-1}, \zeta_{0,t-1}, \zeta_{1,t-1})$ and the observed parameters on day t $(S_i^{ex}(t),\ K_i,\ T_i - t)$. Third, we calculate the prediction error: Let the parameter set denoted by $\Phi_{i,t} = \{S_i^{ex}(t), K_i, T_i - t, \sigma_{t-1}, \zeta_{0,t-1}, \zeta_{1,t-1}\}$, the model-implied option price by $\tilde{C}_{i,t}(\Phi_{i,t})$, and market price by $C_{i,t}$. Then, the pricing errors are calculated as follows:

$$\epsilon_{i,t}(\Phi_{i,t}) = \tilde{C}_{i,t}(\Phi_{i,t}) - C_{i,t}.$$

At last, we compare the average prediction error of all four categories.

Following the estimation procedure above, we calculate the daily average SSE to directly compare the out-of-sample pricing performances of the GBS and BS models. Table 6 summarizes the out-of-sample prediction performance regarding the two models' daily average SSE and the GBS model's win ratios for each estimation method. As shown, the SSE of the GBS model is invariably smaller than that of the BS model, which is additional strong evidence of the dominant advantage of the GBS model. The reductions in the pricing error are not as large as in the in-sample fit; however, the win ratios are close to one for each of the four estimation approaches. For example, with the moneyness-based approach, the GBS model outperforms the BS model in 86.35% of the trading days in the test sample, even though the improvement in terms of the SSE is relatively low. In contrast, the GBS model with the maturity-based approach results in a 33% decrease in SSE compared to the BS prediction errors. Finally, the *t*-tests for the mean differences in the SSEs show that the GBS model yields statistically significant smaller prediction errors.

[Insert Table 6 here]

Figure 14 shows the ratio of the daily SSE of the GBS model to that of the BS model to show the relative prediction performances using the four estimation methods. Furthermore, Figure

15 shows the differences between the SSEs of the GBS and BS models with the MM-based estimation across the 24 categories. As a result, the GBS model's out-of-sample prediction error is lower than that of the BS model in most cases, with several exceptions of the deep ITM and OTM options.

[Insert Figure 14 here]

[Insert Figure 15 here]

Table 7 examines the mean squared error of the predictions for each category by the MM-based estimation, where both the GBS and BS models have the lowest SSE in Table 6. Appendix E presents the other approaches' out-of-sample prediction errors for each category. The out-of-sample prediction performance of the GBS model reveals the following findings. First, from Table 7 and Appendix E, the GBS model shows better out-of-sample pricing performances than the BS model in almost all 24 categories, regardless of the estimation method. This outcome demonstrates that the GBS model's improved prediction power is not an overfitting result. Second, the maturity-based and MM-based estimations deliver the best improvement of the GBS model compared to the BS model. This result indicates that we can estimate model parameters more precisely by classifying the option data along maturity, which is consistent with our estimation results in the in-sample fit.

[Insert Table 7 here]

4.4. Implied RN moments

Section 4.1 shows that the BS model suffers from the so-called volatility smile problem. This section investigates if and how the smile shape across option moneyness is mitigated after including the generalization terms in the GBS model. Figure 8 indicates that the BS model-implied volatility function has a U-shape regarding option moneyness; therefore, we assume that both BS and GBS model-implied volatilities are quadratic functions of option moneyness

as follows (Peña et al., 1999):

$$\sigma_i^{implied} = \beta_0 + \beta_1 \ln(S/K) + \beta_2 \{\ln(S/K)\}^2 + \varepsilon_i,$$

where $\sigma_i^{implied}$ is the implied volatility of option i, and S/K represents the moneyness of option i. β_0 is a constant, β_1 represents the slope of the volatility smile, β_2 represents the degree of curvature of the volatility smile, and ε_i is the error term. When we imply volatilities from the GBS model, we fix ζ_0 and ζ_1 to their daily estimates ($\hat{\zeta}_{0,t}$ and $\hat{\zeta}_{1t}$) and solve the following equation for $\tilde{\sigma}$:

$$C_{i,t} = \hat{C}_{GBS}\left(S_i^{ex}(t), K_i, T_i - t, \tilde{\sigma}_t, \hat{\zeta}_{0,t}, \hat{\zeta}_{1t}\right).$$

Here, $C_{i,t}$ and $\hat{C}_{GBS}$ are the actual price and the function of the GBS option price model, respectively. We estimate β_1 and β_2 for each day for both the BS and GBS models. We expect that the GBS model can resolve the volatility smile problem of the BS model; therefore, we hypothesize that β_1 and β_2 of GBS model-implied volatilities are closer to zero than the BS model-implied volatilities.

Table 8 reports the average slopes and degrees of curvature of the volatility smile of the BS model and the four different GBS model fits. The volatilities implied from the GBS model fits still featured smile shapes with a positive slope and degree of curvature; however, the three GBS fits (All option-, Moneyness-, and MM-based fits) resulted in flatter smiles with a less steep slope and less degree of curvature than the BS model's volatility smile. In other words, the GBS model can partially resolve the volatility smile problem in the BS model.

[Insert Table 8 here]

Based on *Proposition 2.2*, we calculate the RN skewness and kurtosis using the GBS model

parameters in all options fits. The daily estimated GBS parameters are too volatile;[17] therefore, we calculated the monthly RN skewness and kurtosis using the estimated GBS parameters for each monthly subsample. The GBS model-implied RN moments may vary across different time-to-maturities; thus, we set the time-to-maturity to 100 days (i.e., $T - t = 100/360$). Figure 16 shows the resulting monthly RN skewness and kurtosis. The results consistently indicate the negative skewness and positive excess kurtosis of the underlying stock returns, which the BS model fails to explain.[18] The GBS model adequately captures the non-Gaussian feature of the underlying stock return, resulting in reduced pricing errors compared to the BS model.

[Insert Figure 16 here]

4.5. GBS parameters and investor sentiment

4.5.1. Validation using past return information

According to our postulation in Section 2.3.2, ζ_0 should be negatively related to RN skewness and positively related to RN kurtosis; ζ_1 should be positively related to RN kurtosis. These RN moments again serve as a proxy for investors' perceptions of future returns and volatility. This fact gives the following empirically testable hypotheses. (1) Estimated ζ_0 should have a negative correlation with the expected future return and a positive correlation with the expected future return volatility. (2) ζ_1 should have a positive correlation with the expected future return volatility. For our empirical investigation, we first calculate the weekly average values of ζ_0 and ζ_1 (ζ_0^w and ζ_1^w hereafter). Investor sentiment is not deemed as volatile as the daily trading data or stock price movements; therefore, we use the weekly

[17] We confirmed that the daily RN skewness and kurtosis calculated using the daily GBS parameters have a similar pattern to the monthly RN skewness and kurtosis; however, they they fluctuate wildly.

[18] We also noted from Figure 16 that RN kurtosis tends to increase during recessions. Accordingly, we examined the correlation between RN kurtosis and the US GDP growth rate and found that the correlation is −0.2221, statistically significant at the 10% level (the *p*-value is 0.0778).

averages. The existing literature usually uses one week or one month as an appropriate period.

In most cases, stock returns exhibit positive autocorrelations (Lo and Mackinlay, 1988). Ample empirical evidence also suggests that investors rely heavily on past performances to form expectations of future returns (Amin et al., 2004); thus, recent returns might serve as the most important determinant of investor sentiment (Brown and Cliff, 2004).[19] Therefore, we choose the historical returns as the proxies of investors' beliefs regarding future return prospects. Specifically, we use the weekly average of daily S&P 500 returns on recent 1, 2, 3, and 4 weeks to determine the expectation of future returns. Moreover, for the expectation of future return volatility, we use the weekly average of daily S&P 500 squared returns on recent 1, 2, 3, and 4 weeks. Table 9 reports (1) the correlation coefficient estimates between ζ_0 and past returns in panel A, (2) those between ζ_0 and past return volatility in panel B, and (3) those between ζ_1 and past return volatility in panel C. All negative correlations between ζ_0 and the historical returns strongly suggest that ζ_0 is significantly related to the investor sentiment captured by past returns. In contrast, ζ_0 and ζ_1 are positively related to the past squared return, which serves as a proxy for the expected future return variance.

[Insert Table 9 here]

To further confirm the postulation in Section 2.3.2, we regress ζ_0 on the historical returns and squared returns of the past 1, 2, 3, and 4 weeks. We also regress ζ_1 on the historical squared returns of the past 1, 2, 3, and 4 weeks. The first-order lag term is included in both regressions to control the potential autocorrelations. Table 10 presents the results. Panel A of Table 10 shows that ζ_0 is negatively related to the investors' expectation of future returns; the coefficients are negative for past returns within the past 4 weeks. When the market has

[19] Amin et al. (2004) demonstrated that the stock market's momentum can impact the option price, and investors' expectations of future returns could be one of the channels.

increased over a specific time, investors are likely to expect the upward trend to continue and become highly bullish. In this situation, they tend to seek to exploit this expectation by buying more calls to speculate, thereby pushing up the call prices[20]; such an effect of positive expectation is reflected in a negative ζ_0. Panel B of Table 10 reports the regression results of ζ_0 on squared historical returns. The results support our interpretation that ζ_0 is positively related to investors' expectations about future return volatility. We also regress ζ_1 on the historical squared returns of the past 1, 2, 3, and 4 weeks. Table 11 documents the regression results, showing that the coefficients are positive for past returns within the past 4 weeks. That is, ζ_1 is also positively related to the investors' expectation of future return volatility. The regression results in Tables 10 and 11 further support our postulation in Section 2.3.2: ζ_0 is negatively related to investors' expectations about future returns, while both ζ_0 and ζ_1 are positively related to those regarding future return volatility.

[Insert Table 10 here]

[Insert Table 11 here]

4.5.2. Validation using well-established sentiment proxies

Finally, we validate our parameter estimations by comparing the estimated ζ_0 and ζ_1 with the investor sentiment survey results from the American Association of Individual Investors (AAII) and the VIX index, respectively. The AAII survey result is given weekly, reflecting investors' opinions on whether the market will be bullish or bearish in the next six months (% value for each opinion is provided). The proportion of bullish investors minus that of bearish investors is used as a proxy of investors' expectations of future return. The VIX index

[20] In line with this reasoning, several studies have proposed demand-based option pricing models that connect buying pressure with the daily changes of implied volatility (Bollen and Whaley, 2004) or the pricing kernel (Garleanu et al., 2009). Garleanu et al. (2009) concluded that when investors anticipate positive expected returns, they take action by longing for more calls, which turns into positive demand pressure.

represents investors' expectations of future return volatility. If our interpretation is correct, ζ_0 should be negatively related to the AAII bull-bear spread, while both ζ_0 and ζ_1 should be positively related to the VIX index.

We averaged the daily VIX index each week to ensure consistency with the AAII survey result before clarifying the relationship between the parameters and the sentiment indexes. In Figure 17, panel (a) plots the time series of ζ_0^w and the AAII bull-bear spread, and panel (b) plots the time series of ζ_0^w and the VIX index. Figure 18 shows the time series of ζ_1^w and the VIX index. Figures 17 and 18 show (1) a significantly negative correlation between the AAII bull-bear spread and ζ_0^w and (2) a significantly positive correlation between the VIX index and both ζ_0^w and ζ_1^w. These outcomes are consistent with our interpretation and previous findings. We conclude that the parameters ζ_0 and ζ_1 in our GBS model capture market sentiments toward the expectation of future returns and return volatility, which is not captured by the BS model. In conclusion, our GBS model significantly improves the BS model by solving its well-known problem of price bias reflecting market sentiments.

[Insert Figure 17 here]

[Insert Figure 18 here]

5. Conclusion

We propose a GBS option pricing model by utilizing the recently obtained generalized solution to the heat equation. We provide the closed-form pricing formula for the model, wherein two newly incorporated parameters are interpreted as implied investor sentiment factors.

Recent research has documented that behavioral factors, particularly investor sentiment, have significant pricing implications in the options market, not just the stock market; however, most papers have attempted to relate investor sentiment to option prices, relying on a purely

empirical approach or studying the association between investor sentiment and specific aspects of the option or its underlying security (e.g., volatility smile and risk-neutral skewness). In contrast, our analytical option pricing formula endogenously incorporates additional terms that, through judicious parametrization, turn into factors related to investor sentiment.

Our empirical results show that our model invariably outperforms the standard BS model regarding both in-sample fit and out-of-sample pricing performances. The analysis based on four subsampling methods representing different option characteristics confirms the following. (1) The pricing errors by the GBS model are consistently lower than those by the BS model for in-sample fit. (2) The GBS model wins the BS model in up to 86.35% of the sample days and reduces up to 33% of the SSE for out-of-sample prediction. Moreover, our results demonstrate that the implied volatility smile slope decreases significantly with the additional parameters in our GBS model, supporting that the GBS model can resolve a significant portion of the BS model's pricing bias.

Our empirical analysis proves that our interpretation of the two additional parameters in our GBS is consistent with the option pricing behavior in the S&P 500 option data. The first implied sentiment factor tends to capture investors' belief about the future return and return volatility prospect, while the second factor is related to their expectation of return volatility. Combining the two factors allows our GBS model to explain the investor sentiment toward future expected return and return volatility; thus, our results reveal a possible mechanism through which investor sentiment directly affects the option price.

Our study focuses on call options, leaving the investor sentiment reflected in put options for future research. The put-call parity tightly links the prices of the call and put options; thus, we expect the put options to give us a similar conclusion. However, it would be interesting to investigate how different characteristics in sentiment might be reflected distinctively in calls

and puts and the investors' heterogeneous responses. Furthermore, this study examines investor sentiment mainly from a time series perspective, looking into how temporal variations in investor sentiment affect option pricing behavior. It would also be interesting to extend our study to investigate the differential impact of investor sentiment across different markets and economic and regulatory conditions. A comparison with other option pricing models for relative pricing and hedging performances will add to the existing literature.

References

Aït-Sahalia, Y., & Lo, A.W. (1998). Nonparametric estimation of the state price densities implicit in financial asset prices. *Journal of Finance*, *53*(2), 499–547.

Aït-Sahalia, Y., & Lo, A.W. (2000). Nonparametric risk management and implied risk aversion. *Journal of Econometrics*, *94*(1–2), 9–51.

Amin, K., Coval, J.D., & Seyhun, H.N. (2004). Index option prices and stock market momentum. *Journal of Business*, *77*(4), 835–874.

Amin, K.I., & Jarrow, R.A. (1991). Pricing foreign currency options under stochastic interest rates. *Journal of International Money and Finance*, *10*(3), 310–329.

Amin, K.I., & Jarrow, R.A. (1992). Pricing options on risky assets in a stochastic interest rate economy. *Mathematical Finance*, *2*(4), 217–237.

Amin, K.I., & Ng, V.K. (1993). Option valuation with systematic stochastic volatility. *Journal of Finance*, *48*(3), 881–910.

Andersen, T.G., Fusari, N., Todorov, V. (2015). The risk premia embedded in index options. *Journal of Financial Economics*, *117*(3), 558–584.

Backus, D., Chernov, M., & Martin, I. (2011). Disasters implied by equity index options. *Journal of Finance*, *66*(6), 1969–2012.

Baele, L., Driessen, J., Ebert, S., Londono, J.M., & Spalt, O.G. (2019). Cumulative prospect theory, option returns, and the variance premium. *Review of Financial Studies*, *32*(9), 3667–3723.

Baker, M., & Wurgler, J. (2006). Investor sentiment and the cross-section of stock returns. *Journal of Finance*, *61*(4), 1645–1680.

Bakshi, G., Cao, C., & Chen, Z. (1997). Empirical performance of alternative option pricing models. *Journal of Finance*, *52*(5), 2003–2049.

Bakshi, G., Kapadia, N., & Madan, D. (2003). Stock return characteristics, skew laws, and differential pricing of individual equity options. *Review of Financial Studies*, *16*(1), 101–143.

Bakshi, G.S., & Chen, Z. (1997a). An alternative valuation model for contingent claims. *Journal of Financial Economics*, *44*(1), 123–165.

Bakshi, G.S., & Chen, Z. (1997b). Equilibrium valuation of foreign exchange claims. *Journal of Finance*, *52*(2), 799–826.

Barberis, N., Shleifer, A., & Vishny, R. (1998). A model of investor sentiment. *Journal of Financial Economics*, *49*(3), 307–343.

Bates, D.S. (1991). The crash of '87: was it expected? Evidence from options markets. *Journal of Finance*, *46*(3), 1009–1044.

Bates, D.S. (1996). Jumps and stochastic volatility: exchange rate processes implicit in Deutsche mark options. *Review of Financial Studies*, *9*(1), 69–107.

Bates, D.S. (2000). Post-'87 crash fears in the S&P 500 futures option market. *Journal of Econometrics*, *94*(1–2), 181–238.

Black, F. & Scholes, M. (1973). Pricing of options and corporate liabilities. *Journal of Political Economy*, *81*(3), 637–654.

Bollen, N.P., & Whaley, R.E. (2004). Does net buying pressure affect the shape of implied volatility functions? *Journal of Finance*, *59*(2), 711–753.

Borland, L. (2002a). Option pricing formulas based on a non-Gaussian stock price model. *Physical Review Letters*, *89*(9), 098701.

Borland, L. (2002b). A theory of non-Gaussian option pricing. *Quantitative Finance*, *2*(6), 415–431.

Borland, L., & Bouchaud, J.P. (2004). A non-Gaussian option pricing model with skew. *Quantitative Finance*, *4*(5), 499–514.

Brennan, M.J. (1979). Pricing of contingent claims in discrete time models. *Journal of Finance*, *34*(1), 53–68.

Brown, G.W., & Cliff, M.T. (2004). Investor sentiment and the near-term stock market. *Journal of Empirical Finance*, *11*(1), 1–27.

Choi, B., & Choi, M.Y. (2018). General solution to the Black-Scholes boundary-value problem. *Physica A*, *509*, 546–550.

Choi, B., Kang, H., & Choi, M.Y. (2017). Emergence of the heavy-tailed distributions from the heat equation. *Physica A*, *470*, 88–93.

Cont, R. (2001). Empirical properties of asset returns: stylized facts and statistical issues. *Quantitative*

Finance, *1*(2), 223.

Corrado, C.J., & Su, T. (1996). Skewness and kurtosis in the S&P 500 index returns implied by option prices. *Journal of Financial Research*, *19*(2), 175–192.

De Long, J.B.D., Shleifer, A., Summers, L.H., & Waldmann, R.J. (1990). Noise trader risk in financial markets. *Journal of Political Economy*, *98*(4), 703–738.

Dumas, B., Fleming, J., & Whaley, R.E. (1998). Implied volatility functions: Empirical tests. *Journal of Finance*, *53*(6), 2059–2106.

Eraker, B. (2004). Do stock prices and volatility jump? Reconciling evidence from spot and option prices. *Journal of Finance*, *59*(3), 1367–1403.

Eraker, B., Johannes, M., & Polson, N. (2003). The impact of jumps in volatility and returns. *Journal of Finance*, *58*(3), 1269–1300.

Garleanu, N., Pedersen, L.H., & Poteshman, A.M. (2009). Demand-based option pricing. *Review of Financial Studies*, *22*(10), 4259–4299.

Han, B. (2008). Investor sentiment and option prices. *Review of Financial Studies*, *21*(1), 387–414.

Heath, D., Jarrow, R., & Morton, A. (1992). Bond pricing and the term structure of interest rates: A new methodology for contingent claims valuation. *Econometrica*, *60*(1), 77–105.

Heston, S.L. (1993). A closed-form solution for options with stochastic volatility with applications to bond and currency options. *Review of Financial Studies* **6**, 327–343.

Heston, S.L., & Nandi, S. (2000). A closed-form GARCH option valuation model. *Review of Financial Studies*, *13*(3), 585–625.

Hull, J., & White, A. (1987). Pricing of options on assets with stochastic volatilities. *Journal of Finance*, *42*(2), 281–300.

Jarrow, R., & Rudd, A. (1982). Approximate option valuation for arbitrary stochastic processes. *Journal of Financial Economics*, *10*(3), 347–369.

Lo, A.W., & Mackinlay, A.C. (1988). Stock market prices do not follow random walks: Evidence from a simple specification test. *Review of Financial Studies*, *1*(1), 41–66.

Lucas, R.E. (1982). Interest rates and currency prices in a two-country world. *Journal of Monetary Economics*, *10*(3), 335–359.

McCauley, J.L., & Gunaratne, G.H. (2003). An empirical model for the volatility of returns and option pricing. *Physica A*, *329*(1–2), 178–198.

Melino, A., & Turnbull, S.M. (1990). Pricing foreign currency options with stochastic volatility. *Journal of Econometrics*, *45*(1–2), 239–265.

Melino, A., & Turnbull, S.M. (1991). Pricing of foreign currency options. *Canadian Journal of Economics*, *24*(2), 251–281.

Merton, R.C. (1973). Theory of rational option pricing. *Bell Journal of Economics*, *4*(1), 141–183.

Miltersen, K.R., & Schwartz, E.S. (1998). Pricing of options on commodity futures with stochastic term structures of convenience yields and interest rates. *Journal of Financial and Quantitative Analysis*, *33*(1), 33–59.

Peña, I., Rubio, G., & Serna, G. (1999). Why do we smile? On the determinants of the implied volatility function. *Journal of Banking and Finance*, *23*(8), 1151–1179.

Polkovnichenko, V., & Zhao, F. (2013). Probability weighting functions implied in options price. *Journal of Financial Economics*, *107*(3), 580–609.

Poteshman, A.M. (2001). Underreaction, overreaction, and increasing bioreaction to information in the options market. *Journal of Finance*, *56*(3), 851–876.

Rubinstein, M. (1976). The valuation of uncertain income streams and the pricing of options. *Bell Journal of Economics*, *7*(2), 407–425.

Scott, L.O. (1987). Option pricing when the variance changes randomly: Theory, estimation, and an application. *Journal of Financial and Quantitative Analysis*, *22*(4), 419–438.

Scott, L.O. (1997). Pricing stock options in a jump-diffusion model with stochastic volatility and interest rates. *Mathematical Finance*, *7*(4), 413–426.

Seo, S.B., & Wachter, J.A. (2019). Option prices in a model with stochastic disaster risk. *Management Science*, *65*(8), 3449–3469.

Shaliastovich, I. (2015). Learning, confidence, and option prices. *Journal of Econometrics*, *187*(1), 18–42.

Sharpe, S.A. (2002). Reexamining stock valuation and inflation: Implications of analysts' earnings forecasts. *Review of Economics and Statistics*, *84*(4), 632–648.

Shleifer, A., & Vishny, R.W. (1997). The limits of arbitrage. *Journal of Finance*, *52*(1), 35–55.

Stein, E.M., & Stein, J.C. (1991). Stock price distributions with stochastic volatility: An analytic approach. *Review of Financial Studies*, *4*(4), 727–752.

Stein, J. (1989). Overreactions in the options market. *Journal of Finance*, *44*(4), 1011–1023.

Wiggins, J.B. (1987). Option values under stochastic volatility: Theory and empirical estimates. *Journal of Financial Economics*, *19*(2), 351–372.

Figures and Tables

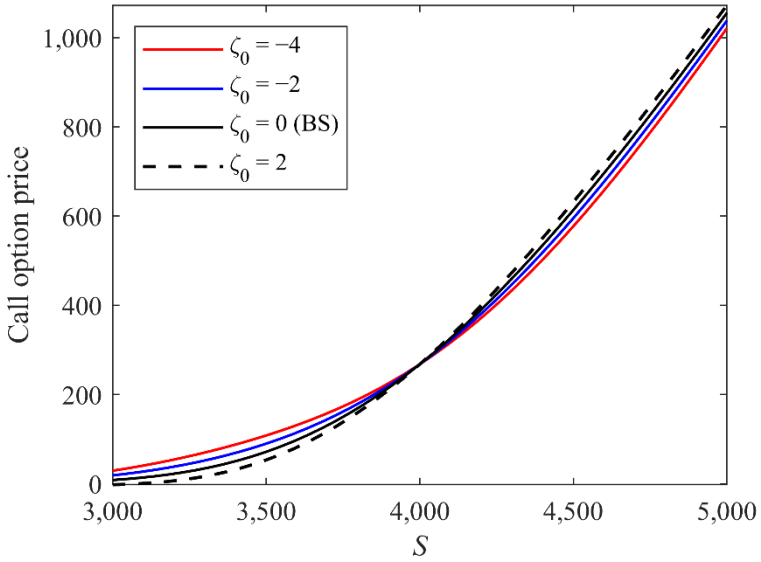

Figure 1. GBS call option prices only including c_1

Note: We set $K = 4000$, $r = 0.03$, $\sigma = 0.3$, $T - t = 100/360$, and S from 3000 to 5000.

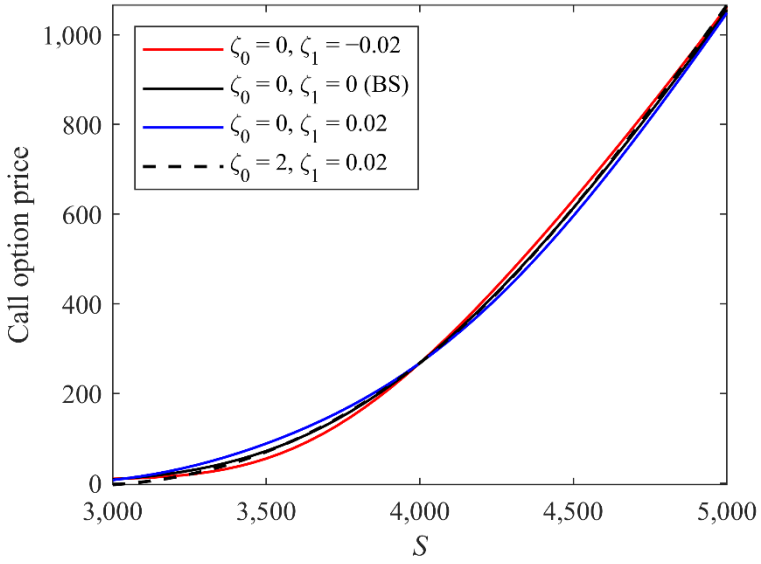

Figure 2. GBS call option prices including c_1 and c_2

Note: We set $K = 4000$, $r = 0.03$, $\sigma = 0.3$, $T - t = 100/360$, and S from 3000 to 5000.

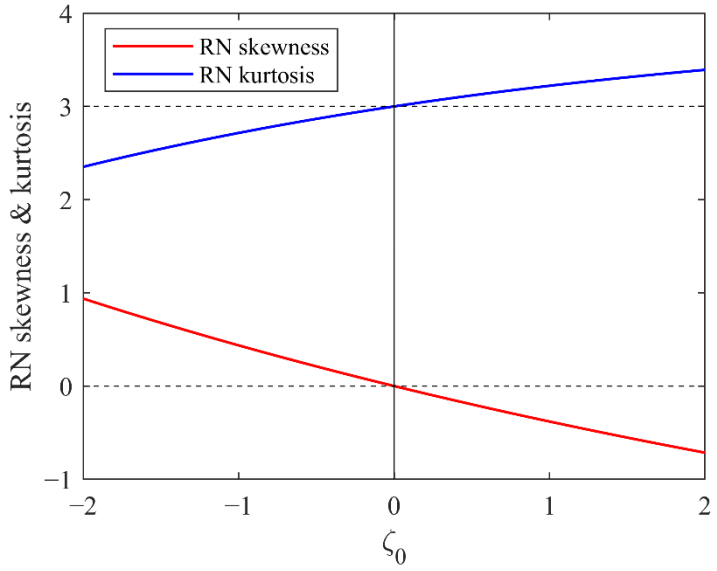

Figure 3. RN skewness and kurtosis vs. ζ_0

Note: We set $S = 4000,\ K = 4000,\ r = 0.03,\ \sigma = 0.3,\ T - t = 100/360$, and $\zeta_1 = 0$.

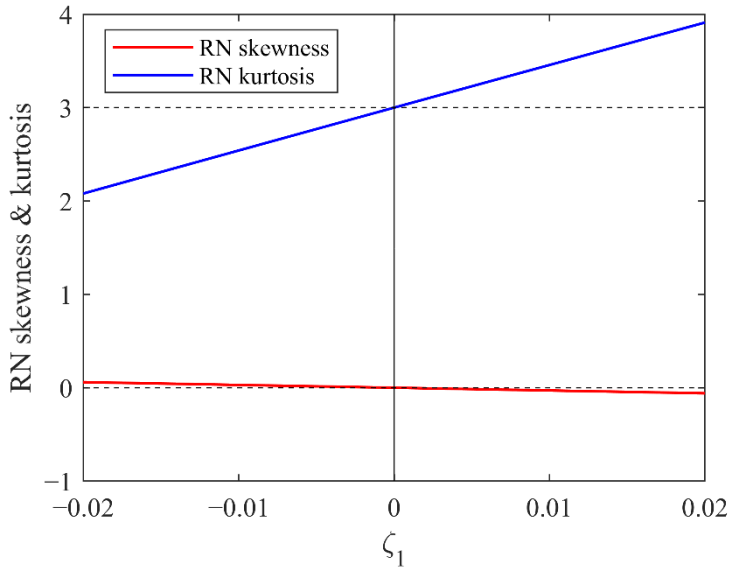

Figure 4. RN skewness and kurtosis vs. ζ_1

Note: We set $S = 4000,\ K = 4000,\ r = 0.03,\ \sigma = 0.3,\ T - t = 100/360$, and $\zeta_0 = 0$.

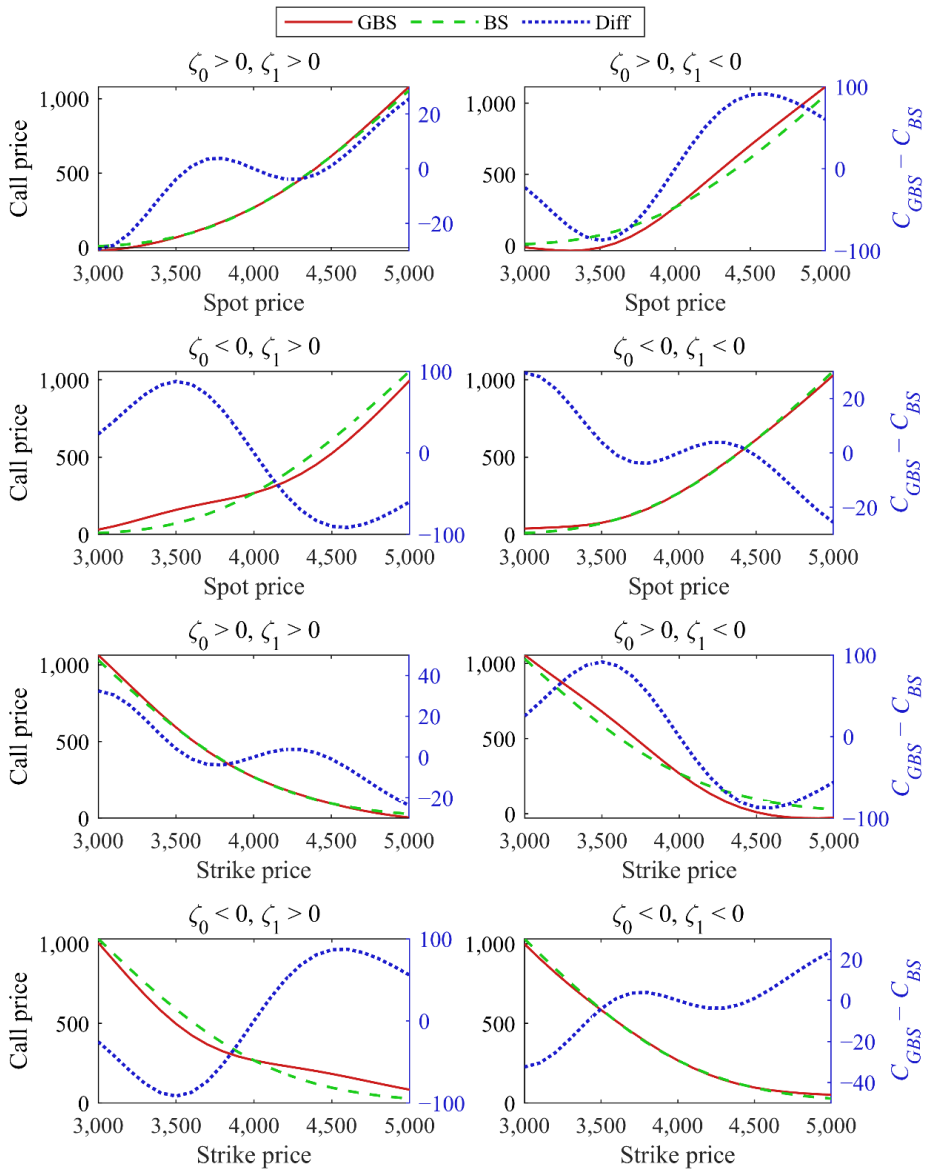

Figure 5. Sensitivity analysis 1

Note: The figure shows the sensitivity of the GBS and BS prices to the spot and strike prices. We hold that $r = 0.03$, $\sigma = 0.3$, and $T - t = 100/360$. In the four figures of the first two rows, we set strike price K to be 4,000 and let spot price S increase from 3,000 to 5,000. In the four figures of the two bottom rows, we set spot price S to be 4,000 and let strike price K increase from 3,000 to 5,000. $\zeta_0 > 0$ and $\zeta_0 < 0$ indicate ζ_0 is set to be 5 and –5, respectively. $\zeta_1 > 0$ and $\zeta_1 < 0$ indicate ζ_1 are set to be 0.05 and –0.05, respectively.

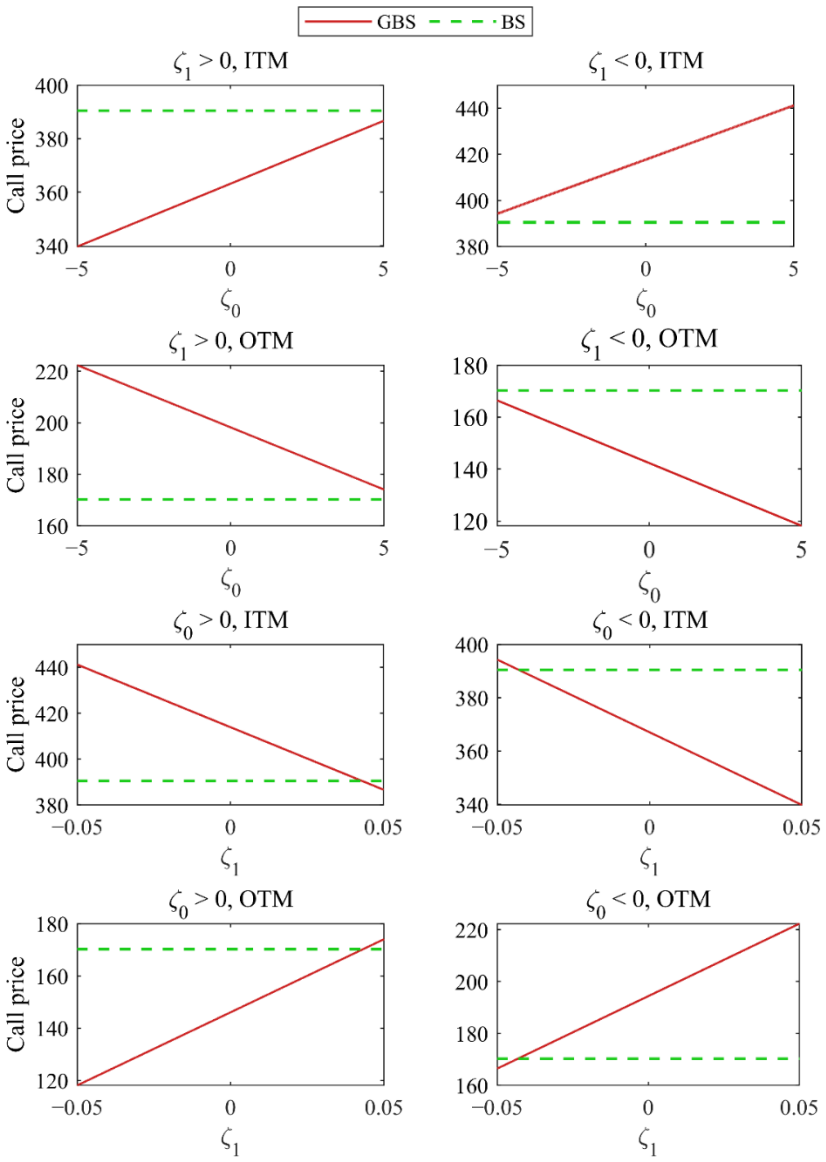

Figure 6. Sensitivity analysis 2

Note: The figure shows the sensitivity of the GBS and BS models to ζ_0 and ζ_1. We hold $K = 4{,}000$, $r = 0.03$, $\sigma = 0.3$, and $T - t = 100/360$. We set $S = 4{,}200$ for ITM and $S = 3{,}800$ for OTM. In the four figures of the first two rows, we set ζ_1 to be 0.05 and –0.05 for $\zeta_1 > 0$ and $\zeta_1 < 0$, respectively, and let ζ_0 increase from –5 to 5. In the four figures of the bottom two rows, we set ζ_0 to be 5 and –5 for $\zeta_0 > 0$ and $\zeta_0 < 0$, respectively, and let ζ_1 increase from –0.05 to 0.05.

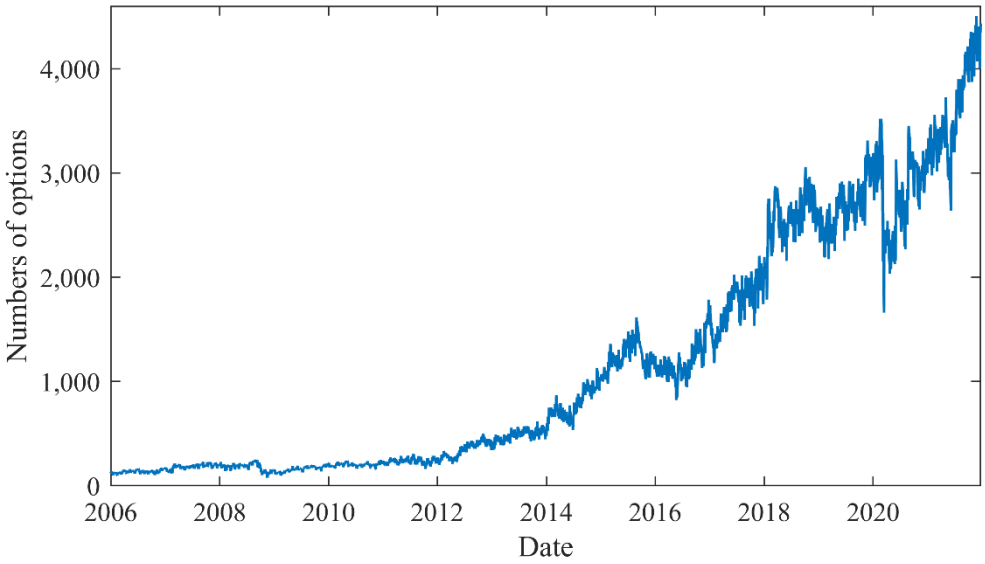

Figure 7. Number of traded call options

Note: The number on each day represents the number of different types of traded call option contracts according to the striking price and time-to-maturity after filtering.

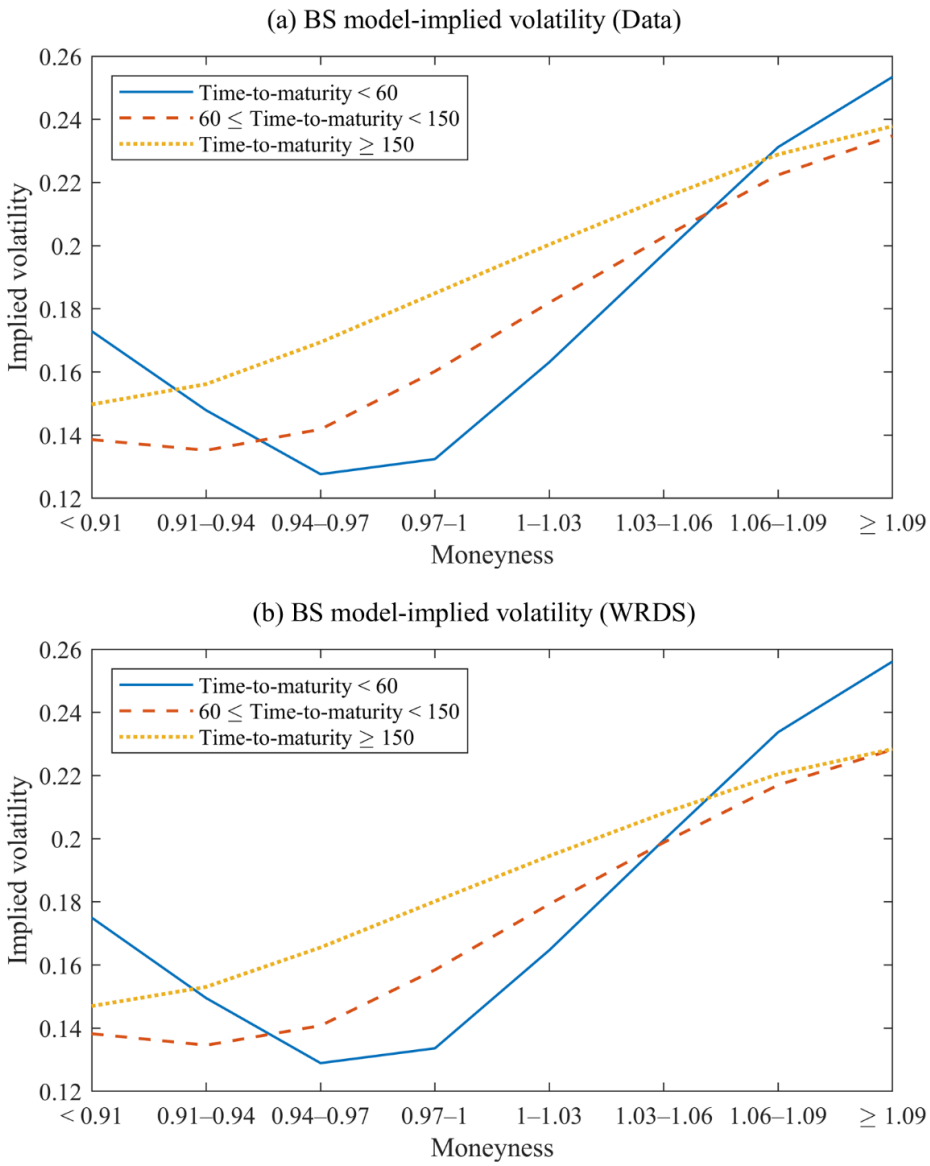

Figure 8. Volatility implied by the BS model

Note: Panel (a) represents the average of the implied volatilities we calculated using the BS model in each category, and panel (b) represents the values given by the WRDS database.

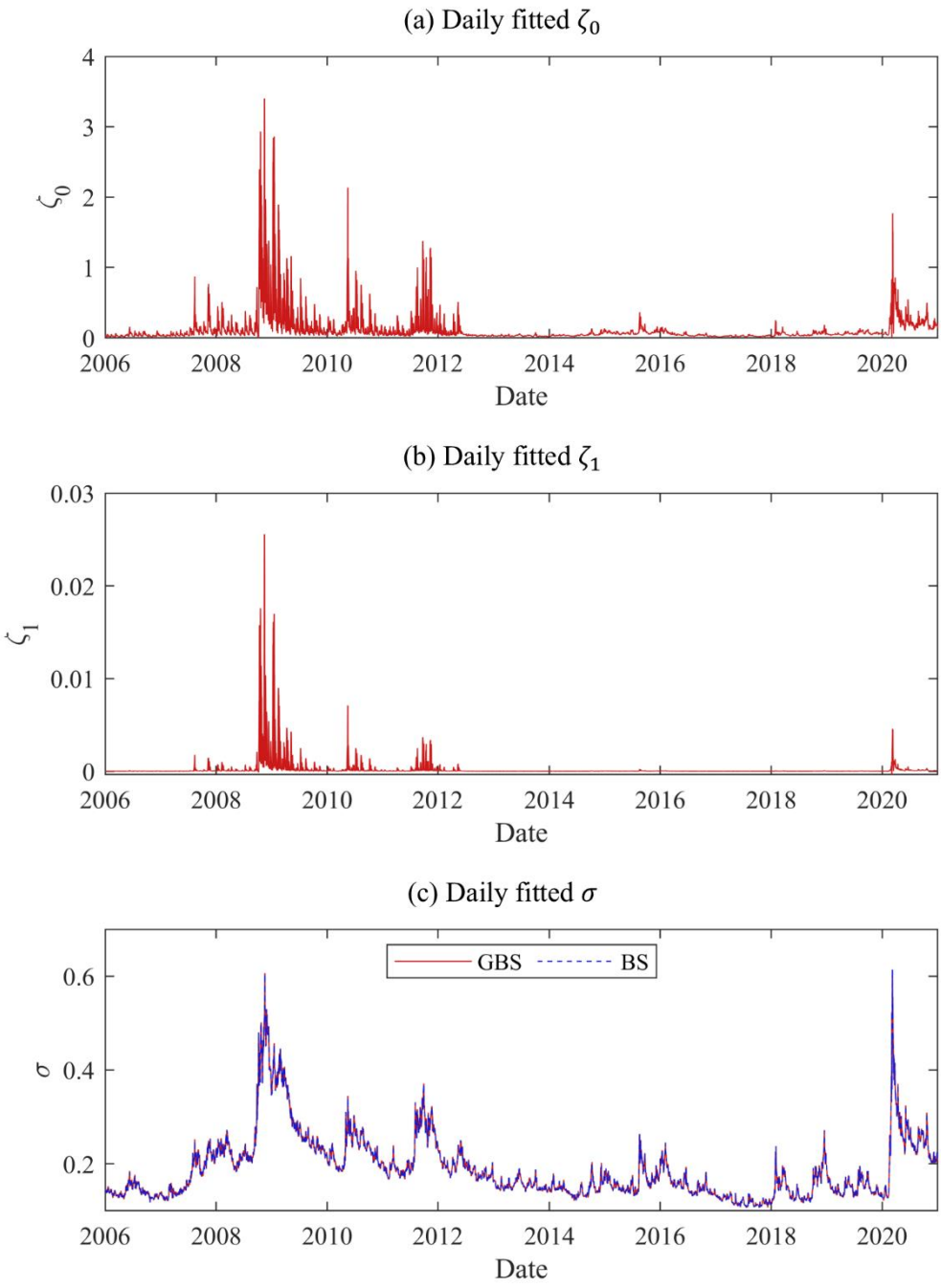

Figure 9. Daily fitted parameters

Note: The parameters are fitted for all option data on each day. Panels (a) and (b) show the time series plot of the daily fitted ζ_0 and ζ_1 in the GBS model, and panel (c) shows the daily fitted σ in the GBS and BS models. The red solid line represents the estimated σ in the GBS model, and the blue dashed line represents the estimated σ in the BS model.

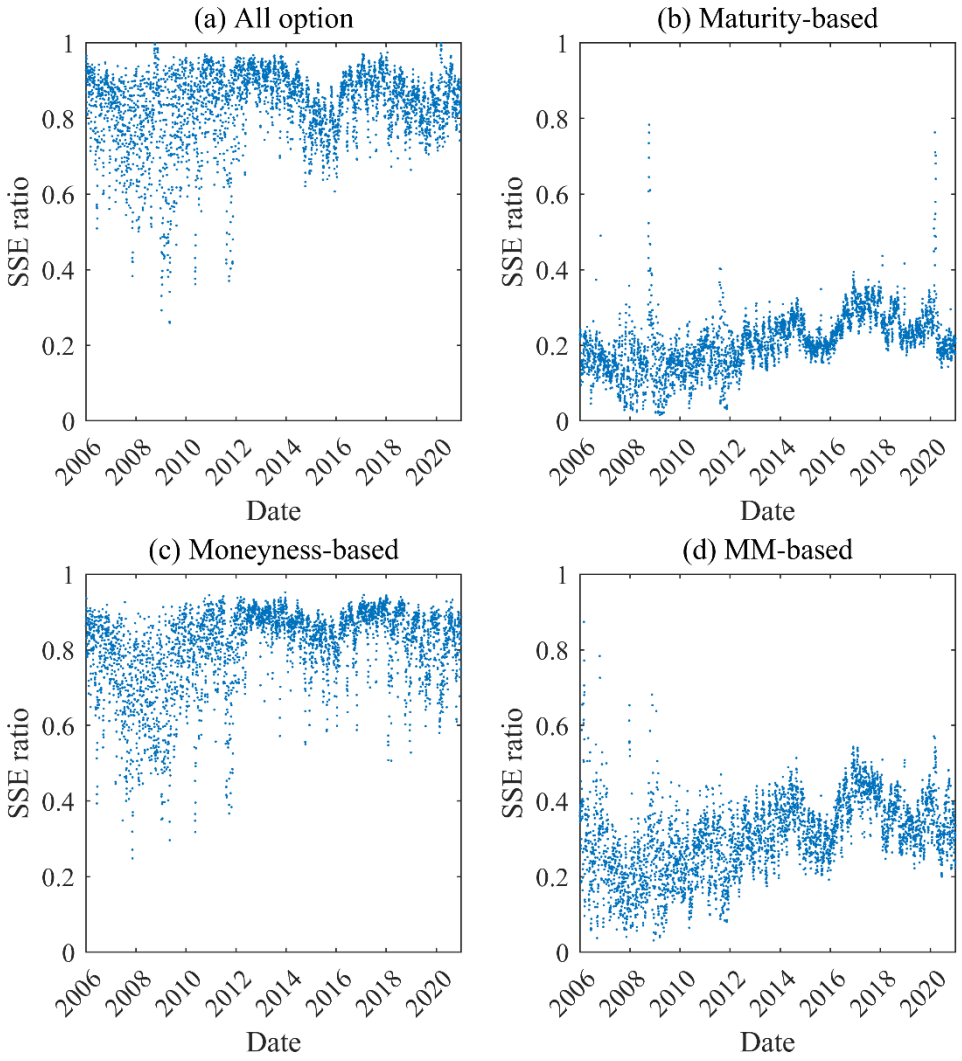

Figure 10. In-sample fit

Note: This figure shows the ratio of the daily average SSE of the GBS model to the BS model. Panel (a) shows the result of all option fits, and panels (b–d) show the results based on the maturity-, moneyness-, and MM-based estimation methods, respectively.

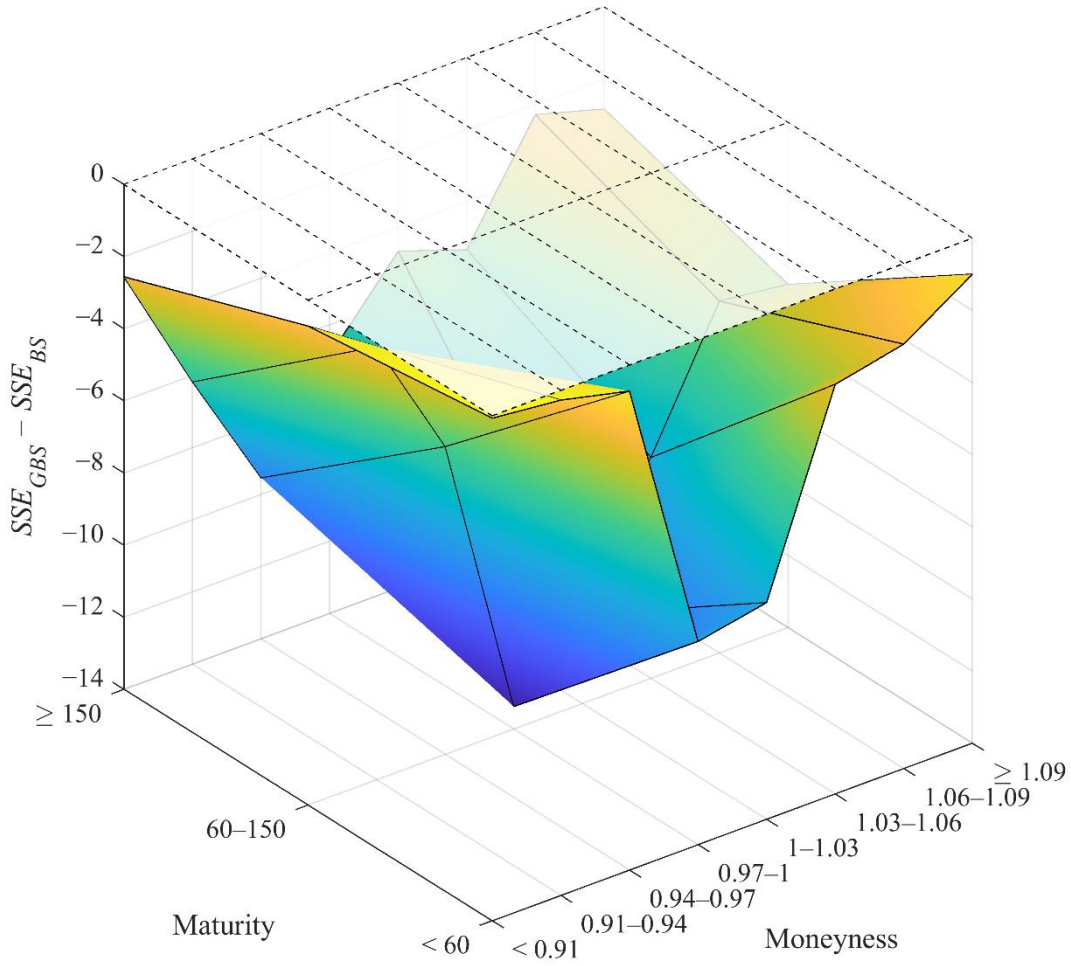

Figure 11. In-sample fit performance based on the MM approach

Note: The GBS and BS models were fitted through the MM-based approach. For each category, we calculated the SSE of the two models and their differences to measure the relative fitness.

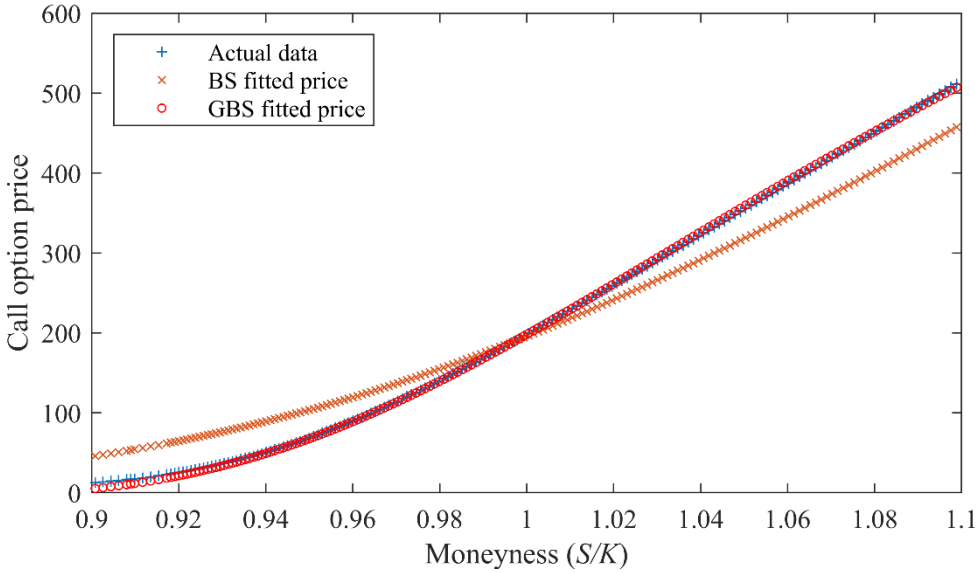

Figure 12. An example of fitting across different moneyness based on the same time-to-maturity

Note: This figure shows the actual, BS-fitted, and GBS-fitted price of the call options traded on December 3, 2021, with time-to-maturity equal to 77 days.

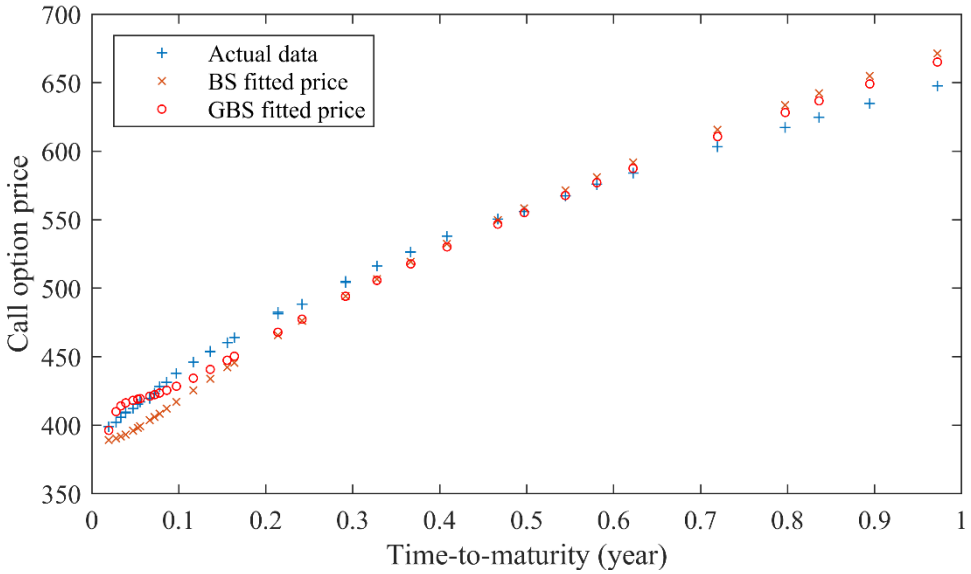

Figure 13. An example of fitting across different time-to-maturity based on the same moneyness

Note: This figure shows the actual, BS-fitted, and GBS-fitted price of call options traded on December 3, 2021, with an exercise price of 4,150 (S&P 500 index is 4,538.43).

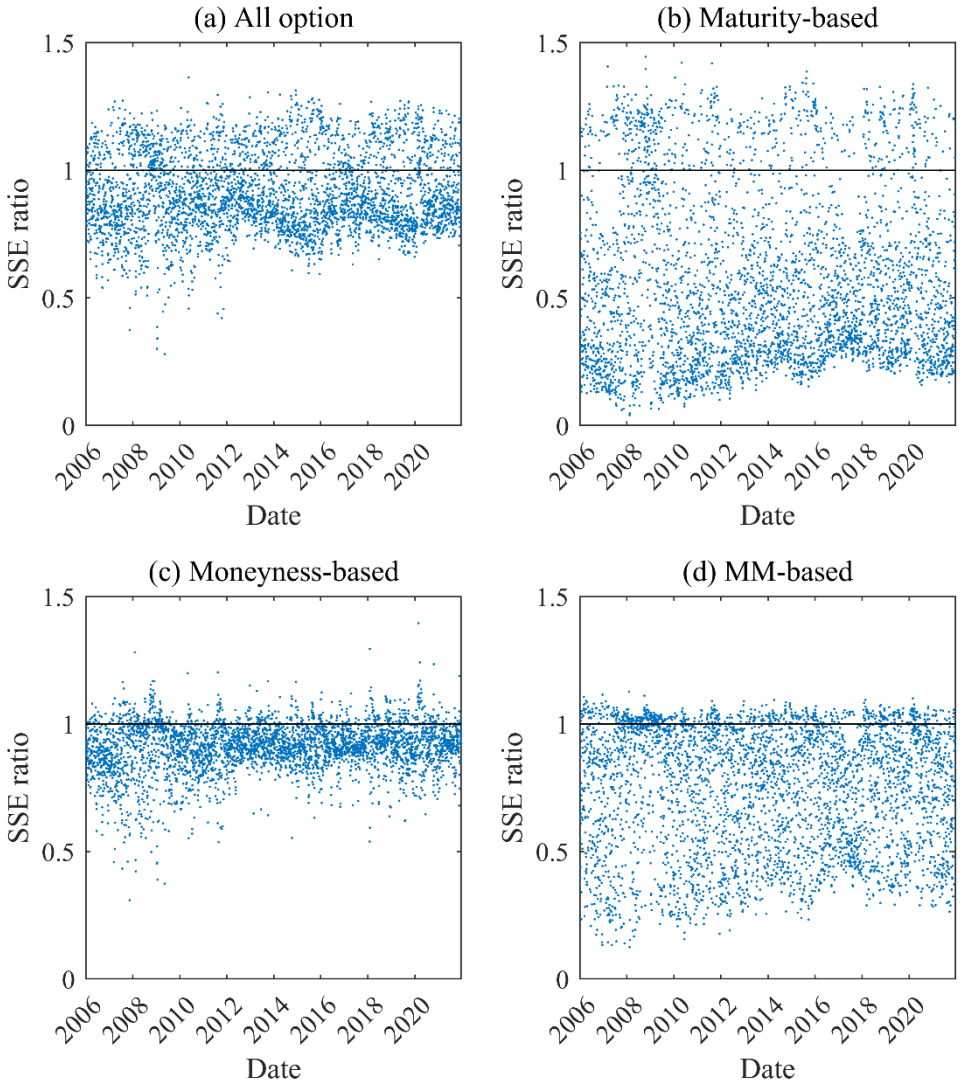

Figure 14. Out-of-sample SSE ratio

Note: This figure shows the ratios of the daily average SSE of the GBS model to that of the BS model. The four panels show the results based on the four estimation results. Panel (a) shows the result of all option fits, and panels (b–d) show the results based on the maturity-, moneyness-, and MM-based estimation methods, respectively.

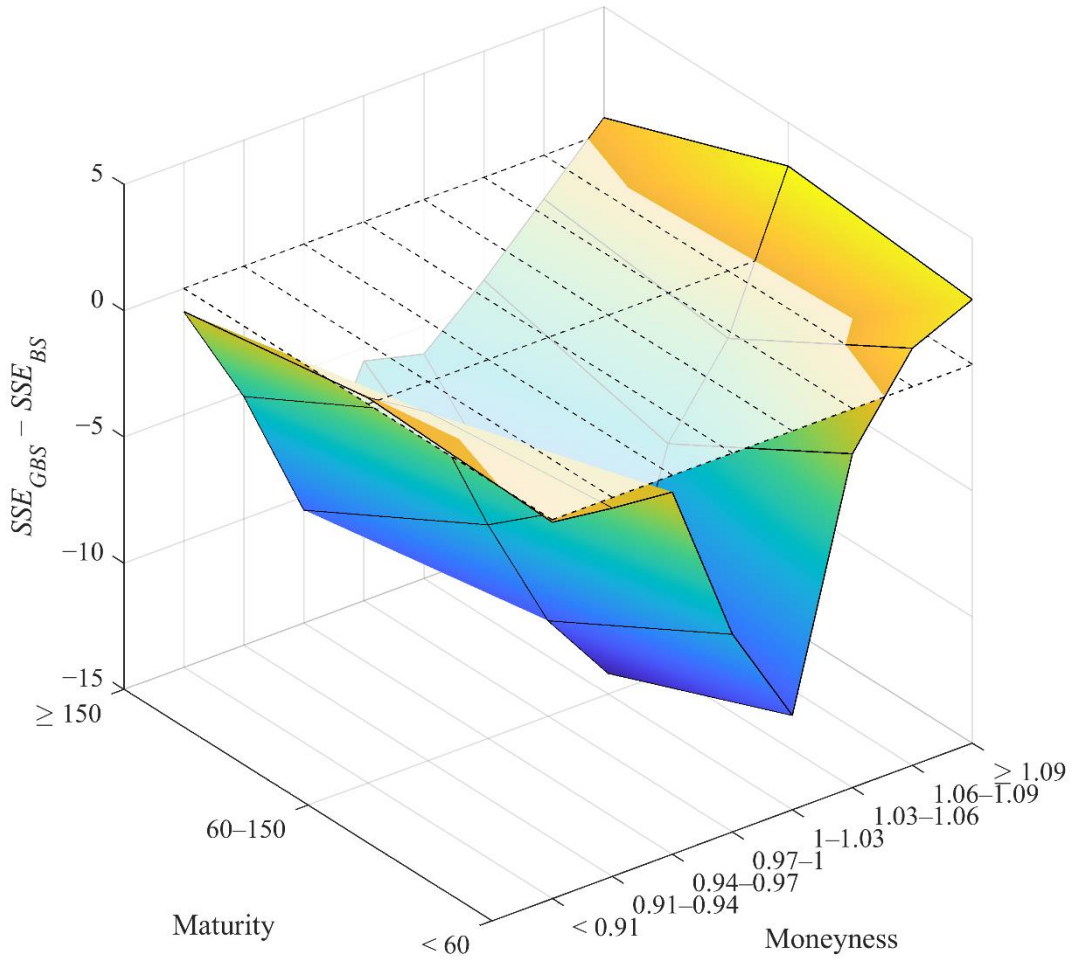

Figure 15. Out-of-sample prediction error based on the MM approach

Notes: The GBS and BS models were fitted through the MM-based approach. We calculate the SSE of the two models for each category and their differences.

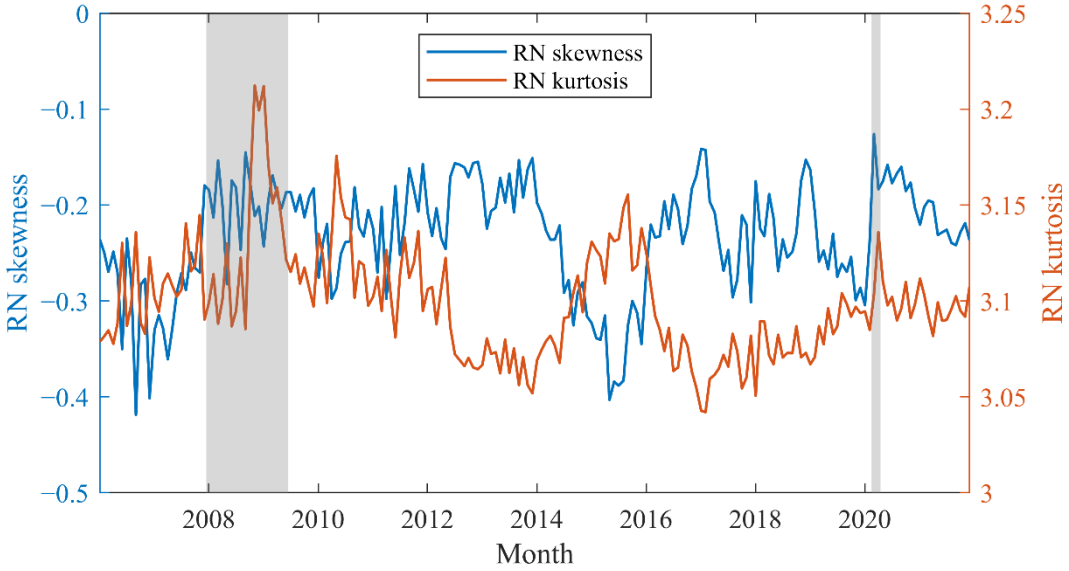

Figure 16. RN skewness and kurtosis implied by the GBS model

Note: The blue and orange solid lines represent the monthly RN skewness and kurtosis, respectively; these are calculated using the monthly estimated parameters in all options fits. We set 100 days to maturity (i.e., $T - t = 100/360$). The shaded areas represent recession periods according to the NBER recession indicator.

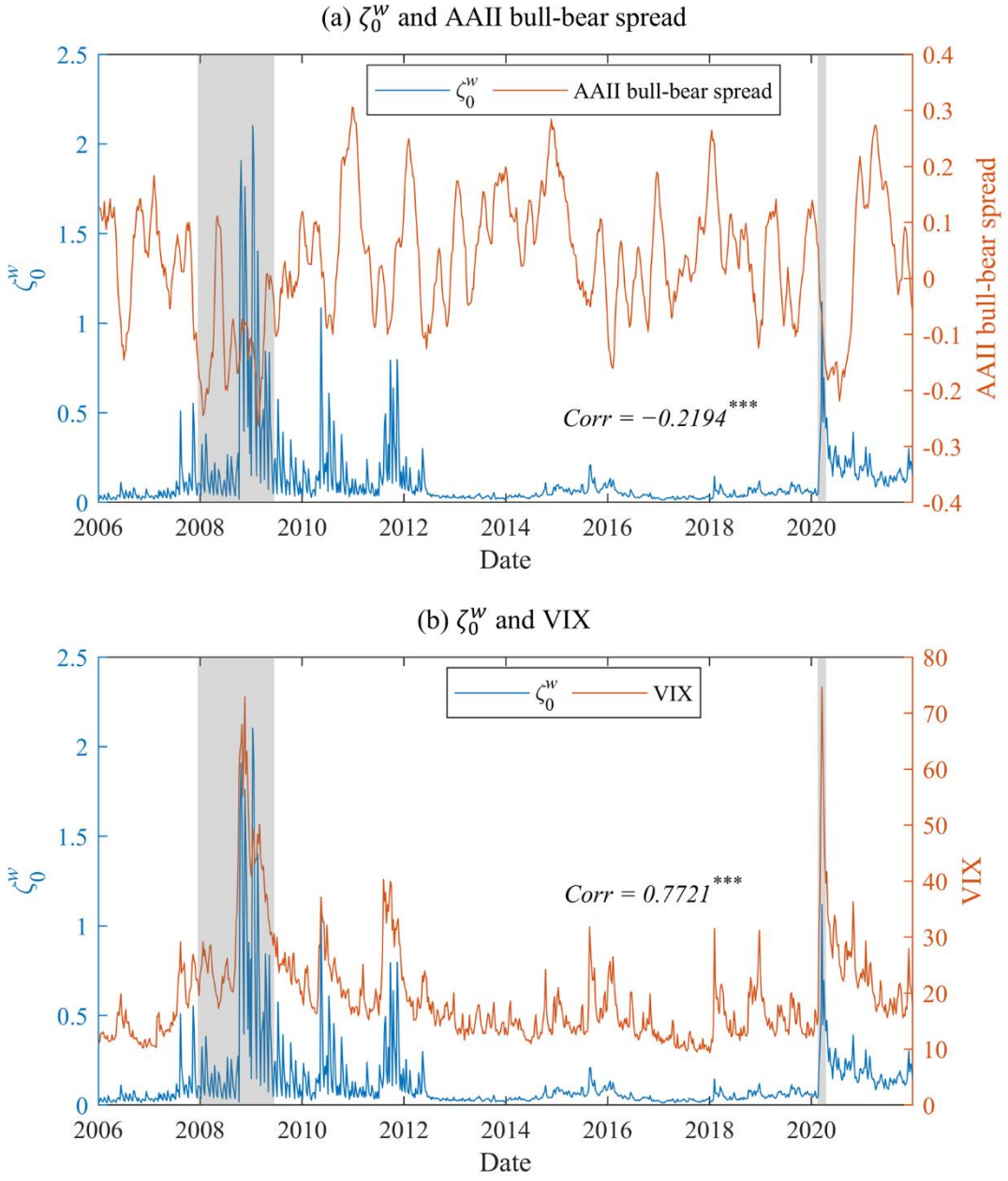

Figure 17. ζ_0^w and investor sentiment

Note: Panel (a) shows the time series of estimated ζ_0^w and the bull-bear spread from the investor sentiment survey by AAII. The AAII bull-bear spread is shown as the 8-week moving average. Panel (b) shows the time series of estimated ζ_0^w and the VIX index. ζ_0^w is the weekly average of the daily estimation of ζ_0. The shaded area indicates the recession period by NBER. *Corr* is the correlation coefficient between ζ_0^w and the sentiment index. *** indicates that the correlation is significant at the 1% level.

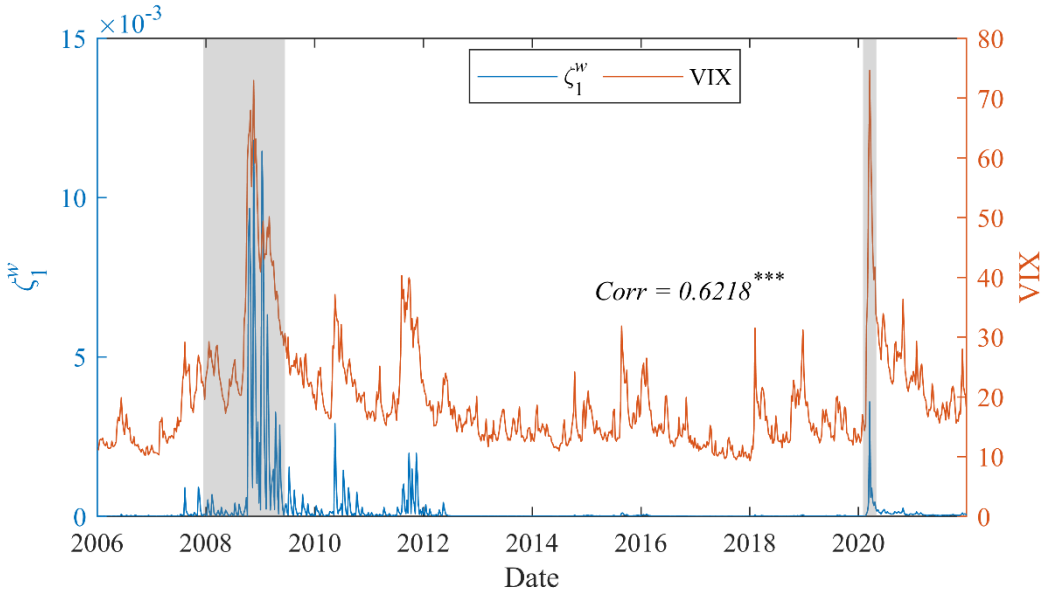

Figure 18. ζ_1^w **and VIX**

Note: This figure shows the time series of estimated ζ_1^w and the VIX index. ζ_1^w is the weekly average of the daily estimation of ζ_1. The shaded area indicates the recession period by NBER. *Corr* is the correlation coefficient between ζ_1^w and the VIX index. *** indicates that the correlation is significant at the 1% level.

Table 1. The main features of our dataset

Feature	Description
Underlying asset	S&P 500 index
Contract type	Call options
Expiration date	Third Friday of every month
Option style	European style
Data source	Wharton Research Data Services (WRDS)

Table 2. Descriptive statistics

Moneyness (S/K)		Time-to-Maturity (days)			Subtotal
		< 60	$60-150$	≥ 150	
OTM	< 0.91	3.14	11.60	45.41	121,350
		(9.87)	(17.59)	(34.95)	
		47,464	48,396	25,490	
	$0.91-0.94$	3.72	18.39	64.15	528,257
		(10.65)	(22.98)	(43.36)	
		256,681	190,432	81,144	
	$0.94-0.97$	7.54	38.77	102.45	770,775
		(14.40)	(34.54)	(56.03)	
		465,146	222,840	82,789	
ATM	$0.97-1$	25.76	78.40	150.76	845,888
		25.22	47.89	69.87	
		545,994	219,589	80,305	
	$1-1.03$	76.14	133.06	205.37	802,221
		(37.82)	(61.61)	(85.64)	
		519,690	206,684	75,847	
ITM	$1.03-1.06$	144.19	194.45	262.73	736,109
		(51.55)	(76.99)	(103.12)	
		470,799	194,081	71,229	
	$1.06-1.09$	214.03	258.71	321.02	649,441
		(69.50)	(94.03)	(121.71)	
		402,748	179,987	66,706	
	≥ 1.09	261.13	302.58	359.75	198,037
		(80.62)	(103.81)	(133.66)	
		120,273	56,693	21,071	
Subtotal		2,828,795	1,318,702	504,581	4,652,078

Note: We divided the sample into 24 categories according to three maturity and eight moneyness. In each category, we calculated the average prices in US dollars (in the first row), standard deviations of the price (in the parenthesis), and the total number of observations (in the third row).

Table 3. Average BS implied volatility

Implied volatility (%)		Time-to-Maturity (days)		
Moneyness (S/K)		< 60	$60-150$	≥ 150
OTM	< 0.91	17.29	13.86	14.97
	$0.91-0.94$	14.79	13.52	15.62
	$0.94-0.97$	12.76	14.19	16.94
ATM	$0.97-1$	13.24	16.02	18.49
	$1-1.03$	16.31	18.20	20.04
ITM	$1.03-1.06$	19.74	20.27	21.51
	$1.06-1.09$	23.12	22.24	22.89
	≥ 1.09	25.34	23.48	23.79

Note: This table shows the BS implied volatility in each of the 24 categories. We estimated the implied volatilities of all the options on each trading day. We then pooled all the implied volatilities together and divided them into 24 categories. Finally, we calculate the mean of the implied volatility within each category.

Table 4. Estimated parameters: All options fit

Parameters		σ (%)	ζ_0	ζ_1	*SSE*
BS	Average	18.89	-	-	260,889
	Std. dev.	6.65	-	-	572,690
GBS	Average	18.92	0.1253	0.0002	225,527
	Std. dev.	6.67	0.2433	0.0012	505,867

Note: The table shows the daily average, standard deviation of the parameters, and average SSE. We estimate the parameters daily using all available option prices each day.

Table 5. In-sample fit performance

SSE	All	Maturity	Moneyness	MM
BS	260,889	215,630	95,025	43,256
GBS	225,527	49,056	79,609	15,138
Change	−13.55%	−81.09%	−14.21%	−65.01%
Win ratio	100%	100%	100%	100%

Note: This table shows the average SSE of the GBS and BS models using the four estimation methods. GBS–BS shows the difference between the average SSE of GBS and BS. The win ratio shows the fraction of dates for which the SSE of the GBS model is smaller than that of the BS model.

Table 6. Out-of-sample prediction performance

SSE	All options	Maturity	Moneyness	MM
BS	473,420	432,525	329,590	282,816
GBS	441,798	290,566	317,879	260,743
Win ratio	72.69%	84.68%	86.35%	84.91%
t-test	−11.1042***	−20.2652***	−8.2139***	−19.4273***

Note: This table shows the daily average SSE of out-of-sample prediction using four different estimation methods; *t*-tests for mean differences of the SSE show that the GBS model yields statistically significant smaller prediction errors than the BS model. *** denotes significance at the 1% level.

Table 7. Out-of-sample prediction error with MM-based estimation

Mean squared error		BS			GBS		
Overall sample		261.6784			241.2546		
Time-to-Maturity (days)		< 60	$60-150$	≥ 150	< 60	$60-150$	≥ 150
OTM	< 0.91	36.12	37.17	127.49	33.18	43.86	81.08
	$0.91-0.94$	32.18	51.92	154.11	30.37	45.36	87.99
	$0.94-0.97$	54.11	124.82	294.30	52.61	95.33	165.31
ATM	$0.97-1$	146.14	229.43	318.53	132.44	178.17	248.33
	$1-1.03$	329.28	339.02	398.78	306.62	270.18	316.41
ITM	$1.03-1.06$	439.53	362.31	381.29	435.51	331.35	322.51
	$1.06-1.09$	508.16	386.36	367.91	512.38	371.00	340.41
	≥ 1.09	454.72	304.42	294.48	488.51	389.43	338.50

Note: This table shows the mean squared pricing errors in each category of the BS and GBS models with the MM-based estimation method.

Table 8. Volatility smile slope and degree of curvature

	BS	GBS			
		All options	Maturity	Moneyness	MM
Panel A. Slope of the volatility smile (β_1)					
Average	0.6066	0.1607	0.1324	0.4091	0.3698
t-test	-	−185.3284***	−30.4640***	−108.5189***	−108.5073***
Panel B. Degree of curvature of the volatility smile (β_2)					
Average	3.1798	2.1628	3.3702	2.6869	2.2312
t-test	-	−41.6020***	0.9634	−12.0052***	−34.4983***

Note: This table shows (1) the average slope and (2) the average degree of curvature of the volatility smile of the BS model and the four different GBS model fits. In panel A, the null hypothesis of each *t*-test is that the smile slope of the GBS model with a given estimation method is larger than that of the BS model. In panel B, the null hypothesis of each *t*-test is that the degree of smile curvature of the GBS model with a given estimation method is larger than that of the BS model. *, **, and *** denote significance at the 10%, 5%, and 1% levels, respectively.

Table 9. Correlation coefficients between additional parameters in the GBS and (squared) historical returns

Panel A. ζ_0^w and historical returns					
	ζ_0^w	ret_{1w}	ret_{2w}	ret_{3w}	ret_{4w}
ζ_0^w	1.0000	−0.1555***	−0.1604***	−0.1146***	−0.1221***
ret_{1w}		1.0000	−0.0948***	0.0546	−0.0826**
ret_{2w}			1.0000	−0.0938***	0.0520
ret_{3w}				1.0000	−0.0925***
ret_{4w}					1.0000
Panel B. ζ_0^w and squared historical returns					
	ζ_0^w	ret_{1w}^2	ret_{2w}^2	ret_{3w}^2	ret_{4w}^2
ζ_0^w	1.0000	0.6002***	0.5654***	0.4986***	0.4684***
ret_{1w}^2		1.0000	0.7157***	0.6388***	0.4388***
ret_{2w}^2			1.0000	0.7157***	0.6388***
ret_{3w}^2				1.0000	0.7157***
ret_{4w}^2					1.0000
Panel C. ζ_1^w and squared historical returns					
	ζ_1^w	ret_{1w}^2	ret_{2w}^2	ret_{3w}^2	ret_{4w}^2
ζ_1^w	1.0000	0.5308***	0.4798***	0.4088***	0.3806***

Note: Panel A presents the correlation matrix among the estimated ζ_0 and historical returns. ζ_0^w denotes weekly average ζ_0. ret_{1w}, ret_{2w}, ret_{3w}, and ret_{4w} denote past recent returns of 1, 2, 3, and 4 weeks, respectively. Panel B presents the correlation matrix among the estimated ζ_0 and historical squared returns. ret_{1w}^2, ret_{2w}^2, ret_{3w}^2, and ret_{4w}^2 denote past recent returns of 1, 2, 3, and 4 weeks, respectively. Panel C presents the correlation coefficients between ζ_1 and historical squared returns. ζ_1^w denotes weekly average ζ_1. *, **, and *** denote significance at the 10%, 5% and 1% levels, respectively.

Table 10. Regression results of ζ_0^w on (squared) historical returns

Panel A. Regression results of ζ_0^w on historical returns				
ζ_0^w	(1)	(2)	(3)	(4)
ind_1	−4.3328***	−2.4201**	−0.4573	−1.5569
	(−4.1109)	(−2.2498)	(−0.4249)	(−1.4600)
ind_1_lag	−2.8324***	−0.5376	−1.8882*	2.6092**
	(−2.6634)	(−0.4995)	(−1.7634)	(2.4453)
$\zeta_0^w\_lag$	0.6594***	0.6679***	0.6720***	0.6824***
	(25.7045)	(25.5010)	(25.7981)	(26.4492)
$(Intercept)$	0.0461***	0.0432***	0.0424***	0.0397***
	(7.1895)	(6.6374)	(6.5310)	(6.1520)
Obs.	830	830	830	830
Adj. R^2	0.4732	0.4626	0.4613	0.4651
Panel B. Regression results of ζ_0^w on squared historical returns				
ζ_0^w	(5)	(6)	(7)	(8)
ind_2	105.1865***	83.8860***	19.4372	57.5748***
	(7.0637)	(5.3961)	(1.2575)	(3.8963)
ind_2_lag	49.7715***	23.9303	78.6436***	59.5284***
	(3.3239)	(1.5928)	(5.3377)	(4.0130)
$\zeta_0^w\_lag$	0.4894***	0.5483***	0.5800***	0.5636***
	(15.7390)	(17.4753)	(19.5035)	(19.7497)
$(Intercept)$	0.0391***	0.0394***	0.0370***	0.0360***
	(6.503)	(6.3691)	(5.9657)	(5.8459)
Obs.	830	830	830	830
Adj. R^2	0.5171	0.4895	0.4892	0.4980

Note: Panel A shows the regression results of ζ_0 on (squared) historical returns. ζ_0^w denotes weekly average ζ_0, ind_1 denotes ret_{1w}, ret_{2w}, ret_{3w} and ret_{4w} for columns (1), (2), (3), and (4), respectively, and the first-order lag terms are introduced to remove autocorrelation. The *t*-statistics are reported in parentheses. Panel B shows the regression results of ζ_0 on historical squared returns. ind_2 denotes ret_{1w}^2, ret_{2w}^2, ret_{3w}^2 and ret_{4w}^2 for columns (5), (6), (7), and (8), respectively. The first-order lag terms are introduced to remove autocorrelation; *t*-statistics are reported in parentheses. *, **, and *** denote significance at the 10%, 5% and 1% levels, respectively.

Table 11. Regression results of ζ_1^w on squared historical returns

ζ_1^w	(1)	(2)	(3)	(4)
ind_2	0.4224***	0.3467***	0.0161	0.1511**
	(5.7851)	(4.6397)	(0.2178)	(2.1477)
ind_2_lag	0.1762**	0.0519	0.3630***	0.4049***
	(2.4440)	(0.7183)	(5.1028)	(5.7136)
$\zeta_1^w\_lag$	0.4800***	0.5326***	0.5601***	0.5269***
	(15.1350)	(16.9639)	(18.7409)	(18.4317)
$(Intercept)$	1.5212e−05	3.6479e−05	3.3750e−05	1.2236e−05
	(0.5532)	(1.3008)	(1.2056)	(0.4454)
Obs.	830	830	830	830
Adj. R^2	0.4361	0.4136	0.4167	0.4389

Note: This table shows the regression results of ζ_1 on squared historical returns. ζ_1^w denotes weekly average ζ_1, ind_2 denotes ret_{1w}^2, ret_{2w}^2, ret_{3w}^2, and ret_{4w}^2 for columns (1), (2), (3) and (4), respectively. The first-order lag terms are introduced to remove autocorrelation; *t*-statistics are reported in parentheses. *, **, and *** denote significance at the 10%, 5% and 1% levels, respectively.

Appendix

Appendix A. Solution of the BS model

Assume the price of the underlying asset is represented by S and follows

$$dS = \mu S dt + \sigma S dW,$$

where μ is the drift term, and σ is the volatility of the underlying assets' return. According to Itô's Lemma,

$$dC = \left(\frac{\partial C}{\partial S}\mu S + \frac{\partial C}{\partial t} + \frac{1}{2}\frac{\partial^2 C}{\partial S^2}\sigma^2 S^2\right)dt + \frac{\partial C}{\partial S}\sigma S dW,$$

where C is the price of the call option. We construct a portfolio, Π, in which we short one share of the call option and long $\frac{\partial C}{\partial S}$ shares of the underlying assets:

$$\Pi = -C + \frac{\partial C}{\partial S}S.$$

With a slight change of time, dt, the value of this portfolio is

$$d\Pi = -dC + \frac{\partial C}{\partial S}dS = \left(-\frac{\partial C}{\partial t} - \frac{1}{2}\frac{\partial^2 C}{\partial S^2}\sigma^2 S^2\right)dt.$$

The return of this portfolio should be equal to the risk-free rate; otherwise, an opportunity for arbitrage arises. Thus, we obtain the following partial differential equation:

$$\frac{\partial C}{\partial t} + \frac{1}{2}\sigma^2 S^2\frac{\partial^2 C}{\partial S^2} + rS\frac{\partial C}{\partial S} - rC = 0, \tag{10}$$

with the boundary condition

$$C(T, S) = \max(S - K, 0).$$

Let

$$S = Ke^x,$$

$$t = T - \frac{2\upsilon}{\sigma^2},$$

$$C(t, S) = KV(\upsilon, x),$$

and change the variables in Eq. (10). Then, we obtain

$$\frac{1}{2}\sigma^2\frac{\partial^2 V}{\partial x^2} + \left(r - \frac{1}{2}\sigma^2\right)\frac{\partial V}{\partial x} - \frac{1}{2}\sigma^2\frac{\partial V}{\partial t} - rV = 0. \tag{11}$$

After defining $k = \frac{2r}{\sigma^2}$, Eq. (11) is transformed to

$$\frac{\partial V}{\partial t} = \frac{\partial^2 V}{\partial x^2} + (k-1)\frac{\partial V}{\partial x} - kV, \tag{12}$$

and the boundary condition is changed to

$$V(0,x) = \max(e^x - 1, 0).$$

We change the variable again and transform Eq. (12) into the heat equation, for which the solution is already known. Then, we can easily obtain a solution for the call price. Let

$$V(\upsilon, x) = e^{\alpha x + \beta \upsilon} u(\upsilon, x),$$

where α and β will be defined later. Then, Eq. (12) can be transformed to

$$\frac{\partial u}{\partial t} = \frac{\partial^2 u}{\partial x^2} + (2\alpha + k - 1)\frac{\partial u}{\partial x} - [(\alpha + k)(\alpha - 1) - \beta]u.$$

To remove u and $\frac{\partial u}{\partial x}$, let the coefficients be zero, that is,

$$\alpha = -\frac{1}{2}(k-1),$$

$$\beta = -\frac{1}{4}(k+1)^2.$$

Then, the solution of Eq. (12) is

$$V(\upsilon, x) = e^{-\frac{1}{2}(k-1)x - \frac{1}{4}(k+1)^2 \upsilon} u(\upsilon, x),$$

where $u(\upsilon, x)$ satisfies the heat equation

$$\frac{\partial u}{\partial \upsilon} = \frac{\partial^2 u}{\partial x^2}, \qquad -\infty < x < \infty \text{and } \upsilon > 0 \tag{13}$$

with the boundary condition

$$\phi(x) = u(0,x) = \max\left[e^{(1-\alpha)x} - e^{-\alpha x}, 0\right].$$

The solution to the heat equation is

$$u(\upsilon, x) = \frac{1}{\sqrt{4\pi\upsilon}} \int_{-\infty}^{\infty} \phi(y) e^{-\frac{(x-y)^2}{4\upsilon}} dy, \tag{14}$$

where the initial condition is

$$\phi(y) = \max\left[e^{\frac{1}{2}(k+1)y} - e^{\frac{1}{2}(k-1)y}, 0\right]$$

$$= e^{\frac{1}{2}(k+1)y} - e^{\frac{1}{2}(k-1)y}, \qquad \text{for } y > 0.$$

Thus, Eq. (14) is equivalent to

$$u(\upsilon,x)=\frac{1}{\sqrt{4\pi\upsilon}}\int_0^{\infty}\left[e^{\frac{1}{2}(k+1)y}-e^{\frac{1}{2}(k-1)y}\right]e^{-\frac{(x-y)^2}{4\upsilon}}dy.$$

We solve the integral

$$u(\upsilon,x)=e^{\frac{1}{2}(k+1)x+\frac{1}{4}(k+1)^2\upsilon}\mathrm{N}(d_1)-e^{\frac{1}{2}(k-1)x+\frac{1}{4}(k-1)^2\upsilon}\mathrm{N}(d_2),$$

where

$$d_1=\frac{x+(k+1)\upsilon}{\sqrt{2\upsilon}},\qquad d_2=\frac{x+(k-1)\upsilon}{\sqrt{2\upsilon}}.$$

Then,

$$V(\upsilon,x)=e^{x}\mathrm{N}(d_1)-e^{-\tau k}\mathrm{N}(d_2).$$

The final solution of the call option price is

$$C_{BS}(t,S)=S\mathrm{N}(d_1)-Ke^{-r(T-t)}\mathrm{N}(d_2)$$

where d_1 and d_2 can be expressed as

$$d_1=\frac{\ln(S/K)+(r+\sigma^2/2)(T-t)}{\sigma\sqrt{T-t}},$$

$$d_2=\frac{\ln(S/K)+(r-\sigma^2/2)(T-t)}{\sigma\sqrt{T-t}}.$$

Appendix B. Solution of the generalized BS model

The general solution to the heat equation (with four parameters γ, λ, κ, and ω) is

$$\varphi(\upsilon,x)=\gamma u(\upsilon,x)+\lambda\theta(\upsilon,x)+\kappa\eta(\upsilon,x)+\omega\chi(\upsilon,x) \tag{15}$$

where

$$\theta(\upsilon,x)\equiv-\frac{\partial u}{\partial x},\qquad \eta(\upsilon,x)\equiv-\frac{\partial\theta}{\partial x},\qquad \chi(\upsilon,x)\equiv-\frac{\partial\eta}{\partial x}.$$

According to Eq. (14), we can derive

$$u(\upsilon,x)=\Lambda_1-\Lambda_2,$$

$$\theta(\upsilon,x)=-\frac{1}{2}[(k+1)\Lambda_1-(k-1)\Lambda_2],$$

$$\eta(\upsilon,x)=\frac{1}{4}[(k+1)^2\Lambda_1-(k-1)^2\Lambda_2]+\frac{1}{\sqrt{4\pi\upsilon}}e^{-\frac{x^2}{4\upsilon}},$$

$$\chi(\upsilon,x)=-\frac{1}{8}[(k+1)^3\Lambda_1-(k-1)^3\Lambda_2]+\Big(\frac{x}{2\upsilon}-k\Big)\frac{1}{\sqrt{4\pi\upsilon}}e^{-\frac{x^2}{4\upsilon}}$$

where

$$\Lambda_1=e^{\frac{1}{2}(k+1)x+\frac{1}{4}(k+1)^2\upsilon}\mathrm{N}(d_1),\qquad \Lambda_2=e^{\frac{1}{2}(k-1)x+\frac{1}{4}(k-1)^2\upsilon}\mathrm{N}(d_2).$$

To make $\varphi(\tau,x)$ satisfy the boundary condition when $\tau\to 0$, that is,

$$\lim_{\upsilon\to 0}\varphi(\upsilon,x)=\max\Big[e^{\frac{1}{2}(k+1)x}-e^{\frac{1}{2}(k-1)x},0\Big],$$

we must consider three cases: (1) $x>0$, (2) $x<0$, (3) $x=0$.

(i) $x>0$

In this case,

$$\lim_{\upsilon\to 0}d_1=\lim_{\upsilon\to 0}d_2=+\infty,\qquad \lim_{\upsilon\to 0}\mathrm{N}(d_1)=\lim_{\upsilon\to 0}\mathrm{N}(d_2)=1,$$

$$\lim_{\upsilon\to 0}\Lambda_1=e^{\frac{1}{2}(k+1)x},\qquad \lim_{\upsilon\to 0}\Lambda_2=e^{\frac{1}{2}(k-1)x},$$

$$\lim_{\upsilon\to 0}\frac{1}{\sqrt{4\pi\upsilon}}e^{-\frac{x^2}{4\upsilon}}=0,\qquad \lim_{\upsilon\to 0}\Big(\frac{x}{2\upsilon}-k\Big)\frac{1}{\sqrt{4\pi\upsilon}}e^{-\frac{x^2}{4\upsilon}}=0.$$

Thus,

$$\lim_{\upsilon\to 0}\varphi(\upsilon,x)=\Big[\gamma-\frac{\lambda}{2}(k+1)+\frac{\kappa}{4}(k+1)^2-\frac{\omega}{8}(k+1)^3\Big]e^{\frac{1}{2}(k+1)x}$$
$$-\Big[\gamma-\frac{\lambda}{2}(k-1)+\frac{\kappa}{4}(k-1)^2-\frac{\omega}{8}(k-1)^3\Big]e^{\frac{1}{2}(k-1)x}.$$

To satisfy the boundary condition when $x>0$, i.e.,

$$\lim_{\tau\to 0}\varphi(\upsilon,x)=e^{\frac{1}{2}(k+1)x}-e^{\frac{1}{2}(k-1)x},$$

it must be

$$\gamma-\frac{\lambda}{2}(k+1)+\frac{\kappa}{4}(k+1)^2-\frac{\omega}{8}(k+1)^3=1, \tag{16}$$

$$\gamma-\frac{\lambda}{2}(k-1)+\frac{\kappa}{4}(k-1)^2-\frac{\omega}{8}(k-1)^3=1. \tag{17}$$

(ii) $x<0$

In this case,

$$\lim_{\upsilon\to 0}d_1=\lim_{\upsilon\to 0}d_2=-\infty,\qquad \lim_{\upsilon\to 0}\mathrm{N}(d_1)=\lim_{\upsilon\to 0}\mathrm{N}(d_2)=0,$$

$$\lim_{\upsilon\to 0}\Lambda_1 = e^{\frac{1}{2}(k+1)x}, \qquad \lim_{\upsilon\to 0}\Lambda_2 = e^{\frac{1}{2}(k-1)x},$$

$$\lim_{\upsilon\to 0}\frac{1}{\sqrt{4\pi\upsilon}}e^{-\frac{x^2}{4\upsilon}} = 0, \qquad \lim_{\upsilon\to 0}\left(\frac{x}{2\upsilon}-k\right)\frac{1}{\sqrt{4\pi\upsilon}}e^{-\frac{x^2}{4\upsilon}} = 0.$$

Thus,

$$\lim_{\upsilon\to 0}\varphi(\upsilon,x) = 0.$$

That is, when $x < 0$, the boundary condition is satisfied with no constraints posed on the parameters.

(iii) $x = 0$

In this case,

$$\lim_{\upsilon\to 0} d_1 = \lim_{\upsilon\to 0} d_2 = 0, \qquad \lim_{\upsilon\to 0}\mathrm{N}(d_1) = \lim_{\upsilon\to 0}\mathrm{N}(d_2) = \frac{1}{2},$$

$$\lim_{\upsilon\to 0}\Lambda_1 = \frac{1}{2}, \qquad \lim_{\upsilon\to 0}\Lambda_2 = \frac{1}{2},$$

Thus,

$$\lim_{\upsilon\to 0}\varphi(\upsilon,x) = -\frac{\lambda}{2}+\frac{\kappa}{4}\cdot 2k-\frac{\omega}{8}\cdot(3k^2+1)+\lim_{\upsilon\to 0}(\kappa-\omega k)\frac{1}{\sqrt{4\pi\upsilon}}.$$

To satisfy the boundary condition when $x = 0$, i.e., $\lim_{\upsilon\to 0}\varphi(\upsilon,x) = 0$, it must be

$$-\frac{\lambda}{2}+\frac{\kappa}{4}\cdot 2k-\frac{\omega}{8}\cdot(3k^2+1) = 0, \tag{18}$$

$$\kappa-\omega k = 0. \tag{19}$$

Eqs. (16)–(19) provide constraints on the parameters γ, λ, κ, and ω for general solution $\varphi(\upsilon,x)$ to satisfy the boundary condition. Although we have four constraints on four parameters, one constraint is redundant; thus, we have one free parameter. To see this, from Eqs. (18) and (19), we immediately obtain

$$\kappa = k\omega,$$

$$\lambda = \frac{k^2-1}{4}\omega.$$

Putting these relations into Eqs. (16) and (17), the following equations always hold:

$$-\frac{\lambda}{2}(k+1)+\frac{\kappa}{4}(k+1)^2-\frac{\omega}{8}(k+1)^3 = 0,$$

$$-\frac{\lambda}{2}(k-1)+\frac{\kappa}{4}(k-1)^2-\frac{\omega}{8}(k-1)^3=0,$$

which indicates that $\gamma=1$.

In sum, the four parameters introduced to the solution of the generalized heat equation have one degree of freedom. They also have the following relationships:

$$\gamma=1,\qquad \lambda=\frac{k^2-1}{4}\omega,\qquad \kappa=k\omega$$

where ω is a free parameter. The final solution, given the restrictions on the parameters, is

$$\begin{aligned}
&\varphi(\upsilon,x)=\gamma u(\upsilon,x)+\lambda\theta(\upsilon,x)+\kappa\eta(\upsilon,x)+\omega\chi(\upsilon,x)\\
&=\left[\gamma-\frac{\lambda}{2}(k+1)+\frac{\kappa}{4}(k+1)^2-\frac{\omega}{8}(k+1)^3\right]\Lambda_1-\left[\gamma-\frac{\lambda}{2}(k-1)+\frac{\kappa}{4}(k-1)^2-\frac{\omega}{8}(k-1)^3\right]\Lambda_2\\
&\qquad+\left[\kappa+\omega\left(\frac{x}{2\upsilon}-k\right)\right]\frac{1}{\sqrt{4\pi\upsilon}}e^{-\frac{x^2}{4\upsilon}}\\
&=\Lambda_1-\Lambda_2+\frac{\omega x}{2\upsilon}\frac{1}{\sqrt{4\pi\upsilon}}e^{-\frac{x^2}{4\upsilon}}.
\end{aligned}$$

This results in a straightforward form, where the first two terms $\Lambda_1-\Lambda_2$ correspond to the standard BS formula, and an additional term is given by $\frac{\omega x}{2\upsilon}\frac{1}{\sqrt{4\pi\upsilon}}e^{-\frac{x^2}{4\upsilon}}$.

From $\varphi(\upsilon,x)$, we can recover the GBS formula

$$\begin{aligned}
&C_{GBS}(\upsilon,x)=Ke^{-\frac{1}{2}(k-1)x-\frac{1}{4}(k+1)^2\upsilon}\varphi(\upsilon,x)\\
&=Ke^{x}\mathrm{N}(d_1)-Ke^{-\upsilon k}\mathrm{N}(d_2)+K\frac{\omega x}{2\upsilon}\frac{1}{\sqrt{4\pi\upsilon}}e^{-\frac{x^2}{4\upsilon}-\frac{1}{2}(k-1)x-\frac{1}{4}(k+1)^2\upsilon}\\
&=Ke^{x}\mathrm{N}(d_1)-Ke^{-\upsilon k}\mathrm{N}(d_2)+K\frac{\omega x}{2\upsilon}\frac{1}{\sqrt{4\pi\upsilon}}e^{-\frac{[x+(k-1)\upsilon]^2}{4\upsilon}-\upsilon k}\\
&=Ke^{x}\mathrm{N}(d_1)-Ke^{-\upsilon k}\mathrm{N}(d_2)+K\frac{\omega x}{2\upsilon}\frac{1}{\sqrt{4\pi\upsilon}}e^{-\frac{d_2^2}{2}-\upsilon k}.
\end{aligned}$$

Recall that

$$x=\ln(S/K),\qquad \upsilon=\frac{\sigma^2}{2}(T-t),\qquad k=\frac{2r}{\sigma^2}.$$

Thus, through the change of variables, we have

$$C_{GBS}(t,S)=S\mathrm{N}(d_1)-Ke^{-r(T-t)}\mathrm{N}(d_2)+\frac{K\omega\ln(S/K)}{\sigma^2(T-t)}\frac{1}{\sqrt{2\pi\sigma^2(T-t)}}e^{-\frac{d_2^2}{2}-r(T-t)}. \quad (20)$$

Appendix C. Proof of discontinuity of c_k for even k

Note that

$$\lim_{t\to T} c_k(t,S) = \lim_{t\to T} \frac{1}{\left(\sigma\sqrt{T-t}\right)^{k+1}} H_k\left(\frac{\ln(S/K)}{\sigma\sqrt{T-t}}\right)\frac{1}{\sqrt{2\pi}} e^{-\frac{d_2^2}{2}-r(T-t)}.$$

When $S = K$, $\frac{\ln(S/K)}{\sigma\sqrt{T-t}} = 0$ and $\lim_{t\to T} d_2 = 0$; thus,

$$\lim_{t\to T} c_k(t,S) = \frac{1}{\sqrt{2\pi}\sigma^{k+1}} \lim_{t\to T} \frac{1}{\left(\sqrt{T-t}\right)^{k+1}} H_k(0).$$

Recall that the $H_k(\cdot)$ being the probabilist's Hermite polynomials defined as

$$H_k(x) = (-1)^k e^{\frac{x^2}{2}} \frac{d^n}{dx^n} e^{-\frac{x^2}{2}}.$$

We can easily find that when k is even, $H_k(0) \neq 0$, which means $\lim_{t\to T} c_k(t,S) = \infty$. Therefore, for the boundary condition to hold, we can add only c_k with odd k to the BS solution. Then, the general solution of the BS PDE should be

$$C_{GBS}(t,S) = C_{BS}(t,S) + \sum_{k=0}^{\infty} \zeta_k c_{2k+1}(t,S).$$

If we consider the first two terms, we have

$$C_{GBS}(t,S) = C_{BS}(t,S) + \zeta_0 c_1(t,S) + \zeta_1 c_3(t,S)$$

where

$$c_1(t,S) = \frac{1}{\left(\sigma\sqrt{T-t}\right)^2} \frac{\ln(S/K)}{\sigma\sqrt{T-t}} \frac{1}{\sqrt{2\pi}} e^{-\frac{d_2^2}{2}-r(T-t)},$$

$$c_3(t,S) = \frac{1}{\left(\sigma\sqrt{T-t}\right)^4} \left(\left[\frac{\ln(S/K)}{\sigma\sqrt{T-t}}\right]^3 - 3\frac{\ln(S/K)}{\sigma\sqrt{T-t}}\right)\frac{1}{\sqrt{2\pi}} e^{-\frac{d_2^2}{2}-r(T-t)}.$$

Appendix D. Calculation of RN skewness and kurtosis

D.1. BS model-implied RN skewness and kurtosis

Hereafter, let $x = \ln(S/K)$. First, we examine $V(t,\tau)$, which has two components given by

$$V_{BS}^{C} = \int_{S(t)}^{\infty} \frac{2\left[1 - \ln\frac{K}{S(t)}\right]}{K^2} C_{BS}(t, S(t); \tau, K)dK\,, \qquad V_{BS}^{P} = \int_{0}^{S(t)} \frac{2\left[1 + \ln\frac{S(t)}{K}\right]}{K^2} P_{BS}(t, S(t); \tau, K)dK$$

where

$$C_{BS} = S(t)\mathrm{N}(d_1) - Ke^{-r\tau}\mathrm{N}(d_2), \qquad P_{BS} = Ke^{-r\tau}\mathrm{N}(-d_2) - S(t)\mathrm{N}(-d_1),$$

and

$$d_1 = \frac{x + (r + \sigma^2/2)\tau}{\sigma\sqrt{\tau}}, \qquad d_2 = \frac{x + (r - \sigma^2/2)\tau}{\sigma\sqrt{\tau}}.$$

Then,

$$V_{BS}^{C} = \int_{S(t)}^{\infty} \frac{2\left[1 - \ln\frac{K}{S(t)}\right]}{K^2} [S(t)\mathrm{N}(d_1) - Ke^{-r\tau}\mathrm{N}(d_2)]dK$$

$$= \int_{S(t)}^{\infty} \frac{2(1+x)}{S(t)^2 e^{-2x}} [S(t)\mathrm{N}(d_1) - Ke^{-r\tau}\mathrm{N}(d_2)]dS(t)e^{-x}$$

$$= 2\int_{-\infty}^{0} (1+x)e^{x}\mathrm{N}(d_1)dx - 2e^{-r\tau}\int_{-\infty}^{0} (1+x)\mathrm{N}(d_2)dx$$

$$= 2\left[\mathrm{N}(d_1)xe^{x}|_{-\infty}^{0} - \int_{-\infty}^{0} xe^{x}\frac{1}{\sigma\sqrt{2\pi\tau}}e^{-\frac{d_1^2}{2}}dx\right]$$

$$- e^{-r\tau}\left[\mathrm{N}(d_2)(x^2+2x)|_{-\infty}^{0} - \int_{-\infty}^{0} (x^2+2x)\frac{1}{\sigma\sqrt{2\pi\tau}}e^{-\frac{d_2^2}{2}}dx\right].$$

Note that

$$\mathrm{N}(d_1)xe^{x}|_{-\infty}^{0} = \mathrm{N}(d_2)(x^2+2x)|_{-\infty}^{0} = 0,$$

and

$$-\frac{d_1^2}{2} + x = -\frac{d_2^2}{2} - r\tau.$$

Define

$$d_0 \equiv \frac{(r - \sigma^2/2)\tau}{\sigma\sqrt{\tau}} = \left(\frac{r}{\sigma} - \frac{\sigma}{2}\right)\sqrt{\tau}.$$

Then,

$$V_{BS}^{C} = -2e^{-r\tau}\int_{-\infty}^{d_0} x\frac{1}{\sqrt{2\pi}}e^{-\frac{d_2^2}{2}}dd_2 + e^{-r\tau}\int_{-\infty}^{d_0}(x^2+2x)\frac{1}{\sqrt{2\pi}}e^{-\frac{d_2^2}{2}}dd_2$$

$$= e^{-r\tau}\int_{-\infty}^{d_0} x^2\frac{1}{\sqrt{2\pi}}e^{-\frac{d_2^2}{2}}dd_2.$$

Through a similar derivation, we can obtain the other component as

$$V_{BS}^{P} = e^{-r\tau}\int_{d_0}^{\infty} x^2\frac{1}{\sqrt{2\pi}}e^{-\frac{d_2^2}{2}}dd_2.$$

Thus,

$$V_{BS} = V_{BS}^{C} + V_{BS}^{P} = e^{-r\tau}\int_{-\infty}^{\infty} x^2\frac{1}{\sqrt{2\pi}}e^{-\frac{d_2^2}{2}}dd_2.$$

Note that

$$x = \sigma\sqrt{\tau}d_2 - \left(r - \frac{\sigma^2}{2}\right)\tau = \sigma\sqrt{\tau}(d_2 - d_0).$$

Then,

$$V_{BS} = e^{-r\tau}\int_{-\infty}^{\infty} x^2\frac{1}{\sqrt{2\pi}}e^{-\frac{d_2^2}{2}}dd_2$$

$$= e^{-r\tau}\left(\sigma\sqrt{\tau}\right)^2\int_{-\infty}^{\infty}(d_2-d_0)^2\frac{1}{\sqrt{2\pi}}e^{-\frac{d_2^2}{2}}dd_2$$

$$= e^{-r\tau}\left(\sigma\sqrt{\tau}\right)^2(1+d_0^2).$$

The same logic holds in solving $\mu(t,\tau)$, $W(t,\tau)$, and $X(t,\tau)$, which can be derived as follows:

$$\mu_{BS}(t,\tau) = \sigma\sqrt{\tau}d_0,$$

$$W_{BS}(t,\tau) = e^{-r\tau}\left(\sigma\sqrt{\tau}\right)^3(3d_0+d_0^3),$$

$$X_{BS}(t,\tau) = e^{-r\tau}\left(\sigma\sqrt{\tau}\right)^4(3+6d_0^2+d_0^4).$$

Finally, we can solve the implied RN skewness and kurtosis of the BS model as follows:

$$\text{SKEW}(t,\tau) = \frac{e^{r\tau}W(t,\tau) - 3\mu(t,\tau)e^{r\tau}V(t,\tau) + 2\mu(t,\tau)^3}{[e^{r\tau}V(t,\tau) - \mu(t,\tau)^2]^{\frac{3}{2}}}$$

$$= \frac{\left(\sigma\sqrt{\tau}\right)^3[3d_0 + d_0^3 - 3d_0(1+d_0^2) + 2d_0^3]}{\left(\sigma\sqrt{\tau}\right)^3[1+d_0^2-d_0^2]^{\frac{3}{2}}}$$

$$= 0,$$

$$\mathrm{KURT}(t,\tau) = \frac{e^{r\tau}X(t,\tau) - 4\mu(t,\tau)e^{r\tau}W(t,\tau) + 6e^{r\tau}\mu(t,\tau)^2V(t,\tau) - 3\mu(t,\tau)^4}{[e^{r\tau}V(t,\tau) - \mu(t,\tau)^2]^2}$$

$$= \frac{\left(\sigma\sqrt{\tau}\right)^4[3 + 6d_0^2 + d_0^4 - 4d_0(3d_0 + d_0^3) + 6d_0^2(1 + d_0^2) - 3d_0^4]}{\left(\sigma\sqrt{\tau}\right)^4[1 + d_0^2 - d_0^2]^{\frac{3}{2}}}$$

$$= 3.$$

D.2. GBS model-implied RN skewness and kurtosis

To derive the GBS model-implied RN skewness and kurtosis, we first examine $V(t,\tau)$, $W(t,\tau)$, $X(t,\tau)$, and $\mu(t,\tau)$ for the GBS model. Specifically, $V_{GBS}(t,\tau)$ has two components given by

$$V_{GBS}^C = \int_{S(t)}^{\infty} \frac{2\left[1 - \ln\frac{K}{S(t)}\right]}{K^2} C_{GBS}(t,S(t);\tau,K)dK,$$

$$V_{GBS}^P = \int_0^{S(t)} \frac{2\left[1 + \ln\frac{S(t)}{K}\right]}{K^2} P_{GBS}(t,S(t);\tau,K)dK$$

where

$$C_{GBS}(t,S(t);\tau,K) = C_{BS}(t,S(t);\tau,K) + \zeta_0 c_1(t,S(t);\tau,K) + \zeta_1 c_3(t,S(t);\tau,K),$$

$$P_{GBS}(t,S(t);\tau,K) = P_{BS}(t,S(t);\tau,K) + \zeta_0 c_1(t,S(t);\tau,K) + \zeta_1 c_3(t,S(t);\tau,K).$$

Thus, for the GBS model including c_1 and c_3, V is given by

$$V_{GBS}(t,\tau) = V_{GBS}^C(t,\tau) + V_{GBS}^P(t,\tau)$$

$$= V_{BS} + \zeta_0 \int_{S(t)}^{\infty} \frac{2\left[1 - \ln\frac{K}{S(t)}\right]}{K^2} c_1(t,S(t);\tau,K)dK + \zeta_1 \int_{S(t)}^{\infty} \frac{2\left[1 - \ln\frac{K}{S(t)}\right]}{K^2} c_3(t,S(t);\tau,K)dK$$

$$+ \zeta_0 \int_0^{S(t)} \frac{2\left[1 + \ln\frac{S(t)}{K}\right]}{K^2} c_1(t,S(t);\tau,K)dK$$

$$+ \zeta_1 \int_0^{S(t)} \frac{2\left[1 + \ln\frac{S(t)}{K}\right]}{K^2} c_3(t,S(t);\tau,K)dK$$

$$= V_{BS} + \zeta_0 V_1(t,\tau) + \zeta_1 V_3(t,\tau)$$

where V_n for $n = 1,3$ is defined as

$$V_n(t,\tau) = \int_0^{\infty} \frac{2\left[1 + \ln\frac{S(t)}{K}\right]}{K^2} c_n(t,S(t);\tau,K)dK.$$

Similarly, μ, W, and X for the GBS model can be derived as

$$\mu_{GBS}(t,\tau) = \mu_{BS}(t,\tau) + \zeta_0\mu_1(t,\tau) + \zeta_1\mu_3(t,\tau),$$

$$W_{GBS}(t,\tau) = W_{BS}(t,\tau) + \zeta_0 W_1(t,\tau) + \zeta_1 W_3(t,\tau),$$

$$X_{GBS}(t,\tau) = X_{BS}(t,\tau) + \zeta_0 X_1(t,\tau) + \zeta_1 X_3(t,\tau),$$

where μ_n, W_n, and X_n for $n = 1,3$ are defined as

$$\mu_n(t,\tau) = e^{r\tau}\left[-\int_0^\infty \frac{1}{K^2} c_n(t,S(t);\tau,K)dK\right],$$

$$W_n(t,\tau) = -\int_0^\infty \frac{6\ln\frac{S(t)}{K} + 3\left[\ln\frac{S(t)}{K}\right]^2}{K^2} c_n(t,S(t);\tau,K)dK,$$

$$X_n(t,\tau) = \int_0^\infty \frac{12\left[\ln\frac{S(t)}{K}\right]^2 + 4\left[\ln\frac{S(t)}{K}\right]^3}{K^2} c_n(t,S(t);\tau,K)dK.$$

By replacing μ, V, W, and X in Eqs. (6) and (7) with μ_{GBS}, V_{GBS}, W_{GBS}, and X_{GBS}, the RN skewness and kurtosis recovered from the GBS model can be calculated as

$$\text{SKEW}(t,\tau) = \frac{e^{r\tau}W_{GBS}(t,\tau) - 3\mu_{GBS}(t,\tau)e^{r\tau}V_{GBS}(t,\tau) + 2\{\mu_{GBS}(t,\tau)\}^3}{[e^{r\tau}V_{GBS}(t,\tau) - \{\mu_{GBS}(t,\tau)\}^2]^{3/2}}$$

$$\text{KURT}(t,\tau)$$
$$= \frac{e^{r\tau}X_{GBS}(t,\tau) - 4\mu_{GBS}(t,\tau)e^{r\tau}W_{GBS}(t,\tau) + 6e^{r\tau}\{\mu_{GBS}(t,\tau)\}^2V_{GBS}(t,\tau) - 3\{\mu_{GBS}(t,\tau)\}^4}{[e^{r\tau}V_{GBS}(t,\tau) - \{\mu_{GBS}(t,\tau)\}^2]^2}.$$

We can calculate the integrals in μ_n, V_n, W_n, and X_n to derive their simpler expressions. First, after several changes of variables, we derive the following expression of V_1:

$$V_1(t,\tau) = \int_0^\infty \frac{2\left[1 + \ln\frac{S(t)}{K}\right]}{K^2} \frac{\ln\frac{S(t)}{K}}{\left(\sigma\sqrt{\tau}\right)^3}\frac{1}{\sqrt{2\pi}} e^{-\frac{d_2^2}{2} - r\tau}dK$$

$$= \int_0^\infty \frac{2x(1+x)}{\{S(t)\}^2 e^{-2x}\left(\sigma\sqrt{\tau}\right)^3}\frac{1}{\sqrt{2\pi}} e^{-\frac{d_2^2}{2} - r\tau}dSe^{-x}$$

$$= \frac{2e^{-r\tau}}{S(t)\left(\sigma\sqrt{\tau}\right)^3}\frac{1}{\sqrt{2\pi}}\int_{-\infty}^\infty x(1+x)e^x e^{-\frac{d_2^2}{2}}dx.$$

Note that

$$-\frac{d_2^2}{2} + x = -\frac{d_3^2}{2} - r\tau + \sigma^2\tau,$$

where we define

$$d_3 \equiv \frac{x+m}{\sigma\sqrt{\tau}}, \qquad m \equiv \left(r - \frac{3}{2}\sigma^2\right)\tau.$$

Then,

$$V_1(t,\tau) = \frac{2e^{-2(r-\sigma^2/2)\tau}}{S(t)\left(\sigma\sqrt{\tau}\right)^3}\frac{1}{\sqrt{2\pi}}\int_{-\infty}^{\infty} x(1+x)e^{-\frac{d_3^2}{2}}dx.$$

Note that

$$x = \sigma\sqrt{\tau}d_3 - m.$$

After we define

$$h \equiv \frac{e^{-2(r-\sigma^2/2)\tau}}{S(t)\left(\sigma\sqrt{\tau}\right)^2},$$

we can easily calculate the integral as

$$V_1(t,\tau) = 2h\frac{1}{\sqrt{2\pi}}\int_{-\infty}^{\infty}\left(\sigma\sqrt{\tau}d_3 - m\right)\left(1 + \sigma\sqrt{\tau}d_3 - m\right)e^{-\frac{d_3^2}{2}}dd_3$$

$$= 2h\left[\left(\sigma\sqrt{\tau}\right)^2 - m + m^2\right].$$

Similarly, we can obtain the other terms as

$$\mu_1(t,\tau) = e^{r\tau}hm,$$

$$W_1(t,\tau) = 3h\left[-2\left(\sigma\sqrt{\tau}\right)^2 + 3\left(\sigma\sqrt{\tau}\right)^2 m - 2m^2 + m^3\right],$$

$$X_1(t,\tau) = 4h\left[3\left(\sigma\sqrt{\tau}\right)^4 - 9\left(\sigma\sqrt{\tau}\right)^2 m + 6\left(\sigma\sqrt{\tau}\right)^2 m^2 - 3m^3 + m^4\right].$$

Similarly, we can obtain the closed-form expressions of μ_3, V_3, W_3, and X_3 as

$$\mu_3(t,\tau) = \frac{e^{r\tau}hm^3}{\left(\sigma\sqrt{\tau}\right)^4},$$

$$V_3(t,\tau) = \frac{2hm^2}{\left(\sigma\sqrt{\tau}\right)^4}\left[3\left(\sigma\sqrt{\tau}\right)^2 - m + m^2\right],$$

$$W_3(t,\tau) = \frac{3hm}{\left(\sigma\sqrt{\tau}\right)^4}\left[6\left(\sigma\sqrt{\tau}\right)^4 - 6\left(\sigma\sqrt{\tau}\right)^2 m + 7\left(\sigma\sqrt{\tau}\right)^2 m^2 - 2m^3 + m^4\right],$$

$X_3(t,\tau)$

$$= \frac{4h}{\left(\sigma\sqrt{\tau}\right)^4}\left[6\left(\sigma\sqrt{\tau}\right)^6 - 18\left(\sigma\sqrt{\tau}\right)^4 m + 27\left(\sigma\sqrt{\tau}\right)^4 m^2 - 21\left(\sigma\sqrt{\tau}\right)^2 m^3 + 12\left(\sigma\sqrt{\tau}\right)^2 m^4 - 3m^5 + m^6\right].$$

Appendix E. Out-of-sample prediction errors

Tables E1 to E3 show the average out-of-sample pricing error of the two models based on all options, moneyness, and maturity approaches.

Table E1. Out-of-sample prediction error with all options fits

Mean squared error		BS			GBS		
Overall sample		436.8231			407.6454		
Time-to-Maturity (days)		< 60	$60-150$	≥ 150	< 60	$60-150$	≥ 150
OTM	< 0.91	87.31	297.89	535.14	93.95	230.96	487.46
	$0.91-0.94$	103.03	401.81	501.30	94.39	319.66	459.43
	$0.94-0.97$	182.62	414.89	332.12	137.45	347.94	315.75
ATM	$0.97-1$	297.05	278.23	362.30	248.00	260.45	364.97
	$1-1.03$	342.01	315.91	801.12	353.11	309.49	799.11
ITM	$1.03-1.06$	485.42	612.96	1488.01	471.86	564.54	1461.16
	$1.06-1.09$	552.97	869.58	2111.18	525.93	781.62	2054.40
	≥ 1.09	395.46	560.40	1813.73	483.22	503.82	1756.76

Note: This table shows the mean squared pricing errors in each category of the BS and GBS models through option-based estimation methods.

Table E2. Out-of-sample prediction error with moneyness-based estimation

Mean squared error		BS			GBS		
Overall sample		304.1119			293.3064		
Time-to-Maturity (days)		< 60	$60-150$	≥ 150	< 60	$60-150$	≥ 150
OTM	< 0.91	75.74	56.42	76.73	45.88	55.53	69.57
	$0.91-0.94$	64.40	82.47	164.27	44.03	79.96	146.35
	$0.94-0.97$	95.58	134.01	530.57	77.61	131.47	471.06
ATM	$0.97-1$	263.07	242.23	455.91	213.12	226.50	454.51
	$1-1.03$	326.58	334.36	983.24	339.42	321.02	962.94
ITM	$1.03-1.06$	454.10	377.91	425.86	446.62	374.43	388.06
	$1.06-1.09$	485.60	380.30	516.89	505.67	374.60	476.95
	≥ 1.09	420.75	297.91	501.62	493.49	291.60	447.48

Note: This table shows the mean squared pricing errors in each category of the BS and GBS models through the moneyness-based estimation method.

Table E3. Out-of-sample prediction error with maturity-based estimation

Mean squared error		BS			GBS		
Overall sample		399.0894			268.1046		
Time-to-Maturity (days)		< 60	$60-150$	≥ 150	< 60	$60-150$	≥ 150
OTM	< 0.91	54.54	267.42	918.22	61.75	166.73	140.64
	$0.91-0.94$	63.37	352.48	878.77	56.80	89.39	98.31
	$0.94-0.97$	99.47	352.31	533.72	79.10	110.90	196.35
ATM	$0.97-1$	161.61	242.10	292.58	140.67	189.57	260.72
	$1-1.03$	318.14	334.40	446.78	305.36	275.36	311.66
ITM	$1.03-1.06$	537.36	666.51	922.80	486.43	369.60	363.27
	$1.06-1.09$	602.00	925.74	1434.49	564.84	428.58	391.84
	≥ 1.09	422.31	596.83	1171.70	480.95	463.48	503.24

Note: This table shows the mean squared pricing errors in each category of the BS and GBS models through the maturity-based estimation method.